J. Fluid Mech. (2021), *vol*. 929, A17, doi:10.1017/jfm.2021.865

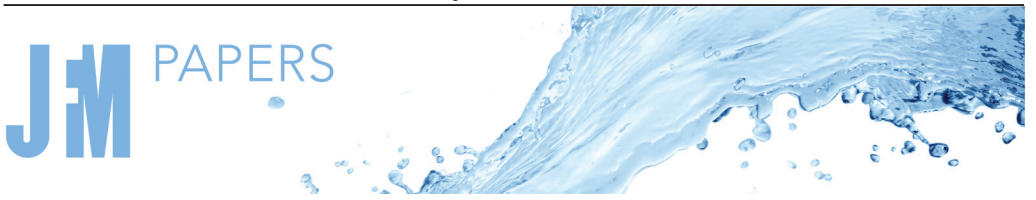

On boundary-layer receptivity to entropy waves

A.I. Ruban[1],†, **S.K. Keshari**[1] **and M.A. Kravtsova**[1]

[1]Department of Mathematics, Imperial College London, 180 Queen's Gate, London SW7 2AZ, UK

(Received 10 April 2021; revised 31 July 2021; accepted 29 September 2021)

In this paper, we consider the generation of the Tollmien–Schlichting waves in the boundary layer on the surface of a wing exposed to entropy waves. It is well known that the free-stream turbulence is composed of two perturbation modes: the vorticity waves and the entropy waves. The receptivity of the boundary layer to the vorticity waves has been studied extensively by various authors. The entropy waves have not attracted such attention. We show that, in high speed subsonic flows, the entropy waves are as important for the receptivity as the vorticity waves. Methodologically, our work relies on the asymptotic analysis of the Navier–Stokes equations at large values of the Reynolds number, which results in the formulation of a suitably modified triple-deck theory. The entropy waves produce oscillations of the gas temperature and density, but the velocity and the pressure remain unperturbed to the leading order. This precludes the entropy waves from penetrating the boundary layer, as happens, for example, with the acoustic waves. Our analysis reveals that the entropy waves decay rapidly in the transition layer that forms near the outer edge of the boundary layer. We find that an entropy wave alone cannot generate the Tollmien–Schlichting waves. However, when the boundary layer encounters a wall roughness, the flow near the roughness appears to be perturbed not only inside the boundary layer but also in the inviscid region outside the boundary layer. The latter comes into the interaction with the density perturbations in the entropy wave. As a result, a localised 'forcing' is created that produces the Tollmien–Schlichting waves. In this paper we present the results of a linear and nonlinear receptivity analysis. We find that the nonlinearity enhances the receptivity significantly, especially when a local separation region forms on the roughness.

Key words: high-speed flow, boundary layer receptivity

1. Introduction

For a passenger airplane in a cruise flight, the flow past the wing represents a classical example of what is referred to as weak turbulence flow. In such flows, the laminar–turbulent transition follows the so-called classical scenario, where the transition is caused by production and amplification of the instability modes. In the flow past an aircraft wing two instability modes are observed, the Tollmien–Schlichting waves and the

† Email address for correspondence: a.ruban@imperial.ac.uk

cross-flow vortices. In addition to the wings, the transition on the nacelles has recently attracted significant attention. This is because modern jet engines have a rather large diameter with the combined circumference of two nacelles being comparable to a wing span. Possible reduction of the viscous drag of a nacelle depends on the success in suppression of the Tollmien–Schlichting waves.

In this presentation we shall assume for simplicity that the boundary layer is two-dimensional with the transition caused by the Tollmien–Schlichting waves. The transition starts with the transformation of the free-stream noise into the Tollmien–Schlichting waves. The receptivity theory serves to describe this process; the main objective being to find the initial amplitude of the Tollmien–Schlichting waves. In the case of low free-stream turbulence, the generated Tollmien–Schlichting waves are weak and cannot lead to immediate transition to turbulence. They have to amplify in the boundary layer before triggering the nonlinear effects, characteristic of the turbulent flow.

The receptivity theory is in a well-advanced stage now, and has been reviewed by a number of authors. Here, we shall give a short account of the results of the theory that are directly related to the analysis in the present paper. For more details, the reader is referred to Ruban, Bernots & Pryce (2013). Our analysis is performed in the framework of the triple-deck theory. When presenting this theory, four papers are usually mentioned as the works where this theory was put forward. Two of these, by Neiland (1969) and Stewartson & Williams (1969), dealt with the boundary-layer separation in a steady supersonic flow, and the other two, by Stewartson (1969) and Messiter (1970), were concerned with the incompressible flow near the trailing edge of a flat plate. However, the fact is that it was Lin (1946) who first discovered the triple-deck model in his analysis of the linear instability of the boundary-layer flow. Lin's conclusion that the triple-deck theory describes the Tollmien–Schlichting waves was later confirmed by Smith (1979).

The first paper, where the triple-deck theory was used to study the receptivity of the boundary layer was published by Terent'ev (1981). In this study, Terent'ev considered an incompressible fluid flow past a flat plate with the steady unperturbed flow given by the Blasius solution. The perturbations were introduced by a short section of the plate surface performing periodic vibrations in the direction perpendicular to the wall. Terent'ev's formulation represented a simplified mathematical model of the classical experiments by Schubauer & Skramstad (1948) where the Tollmien–Schlichting waves were generated by a vibrating ribbon installed inside the boundary layer a small distance from the plate surface. Terent'ev was able to determine the amplitude of the generated Tollmien–Schlichting wave as a function of the amplitude and shape of the vibrating part of the wall.

Experimental studies have shown that some disturbances easily penetrate into the boundary layer and turn into instability modes of the boundary layer, others do not. In the former category are acoustic waves, free-stream turbulence, local and distributed wall roughness, etc. Still, even these perturbations have to satisfy rather restrictive resonance conditions which were first formulated by Kachanov, Kozlov & Levchenko (1982). Unlike in a simple mechanical system, say, a pendulum, where the resonance is observed provided that the frequency of the external forcing is close to the natural frequency of the pendulum oscillations, in fluid flows an effective transformation of external disturbances into instability modes of the boundary layer is only possible if in addition to the frequency, the wavenumber of the external perturbations is in tune with the natural internal oscillations of the boundary layer.

Ruban (1984) and Goldstein (1985) were the first to demonstrate how this double-resonance principle can be used in the receptivity theory. In the 'vibrating ribbon' problem considered by Terent'ev (1981), the two resonance conditions are

satisfied by simply choosing the frequency and the length of the vibrating part of the wall appropriately. The situation is more complex in the case of the boundary-layer receptivity to acoustic noise, which was the subject of the analysis performed by Ruban (1984) and Goldstein (1985). To satisfy the first resonance condition, they assumed the Reynolds number Re to be large and chose the frequency of the acoustic wave to be an $O(Re^{1/4})$ quantity, but since the speed of propagation of acoustic waves is finite, their wavelength appears to be $O(Re^{-1/4})$ long, which is much longer than the wavelength of the Tollmien–Schlichting wave. Hence, the acoustic wave alone is insufficient for the Tollmien–Schlichting wave generation. To satisfy the resonance condition with respect to the wavenumber, the acoustic wave has to come into interaction with a wall roughness, which are, of course, plentiful on a real aircraft wing. Ruban (1984) and Goldstein (1985) demonstrated that the interaction of an acoustic wave with a roughness of $O(Re^{-3/8})$ length does produce Tollmien–Schlichting waves in the boundary layer. An explicit formula for the amplitude of the Tollmien–Schlichting waves was obtained.

Later, Duck, Ruban & Zhikharev (1996) extended the theory to describe the generation of the Tollmien–Schlichting waves by the free-stream turbulence. In incompressible flows, the free-stream turbulence may be modelled as a superposition of vorticity waves. Duck *et al.* (1996) noticed that there is a significant difference in the way the boundary layer interacts with acoustic waves and vorticity waves. The acoustic waves carry pressure perturbations which easily penetrate into the boundary layer and lead to a formation of the Stokes layer near the body surface; this is due to the Stokes layer interaction with steady perturbations near the wall roughness that the Tollmien–Schlichting waves form in the boundary layer. The situation with the vorticity waves is different. They do not carry pressure perturbations and therefore are unable to penetrate the boundary layer. However, a wall roughness produces perturbations not only inside the boundary layer but also in the upper tier of the triple-deck structure that lies outside the boundary layer. The interaction of the steady perturbations in the upper tier with vorticity waves creates the forcing necessary for the Tollmien–Schlichting wave production.

In compressible flows, in addition to vorticity waves the free-stream turbulence also includes the entropy waves. In this paper, we present an asymptotic theory of the boundary-layer receptivity to entropy waves for subsonic flows.

2. Problem formulation

Let us consider a perfect gas flow past a flat plate that is aligned with the mean velocity vector in the free stream; see figure 1. We shall assume that small-amplitude entropy waves are present in the oncoming flow. We shall further assume that there is a small roughness on the plate surface at distance L from the leading edge. In what follows we shall assume that the flow is two-dimensional. To study the flow we use the Cartesian coordinates $(\hat{x}, \hat{y})$, with $\hat{x}$ measured along the flat plate surface from its leading edge O, and $\hat{y}$ in the perpendicular direction. The velocity components in these coordinates are denoted by $(\hat{u}, \hat{v})$. As usual, we denote the time by $\hat{t}$, the gas density by $\hat{\rho}$, pressure by $\hat{p}$, enthalpy by $\hat{h}$ and dynamic viscosity coefficient by $\hat{\mu}$. The 'hat' is used here for dimensional variables. The non-dimensional variables are introduced as follows:

$$\left.\begin{array}{lll} \hat{t} = \dfrac{L}{V_\infty} t, & \hat{x} = Lx, & \hat{y} = Ly, \\ \hat{u} = V_\infty u, & \hat{v} = V_\infty v, & \hat{\rho} = \rho_\infty \rho, \\ \hat{p} = p_\infty + \rho_\infty V_\infty^2 p, & \hat{h} = V_\infty^2 h, & \hat{\mu} = \mu_\infty \mu, \end{array}\right\} \tag{2.1}$$

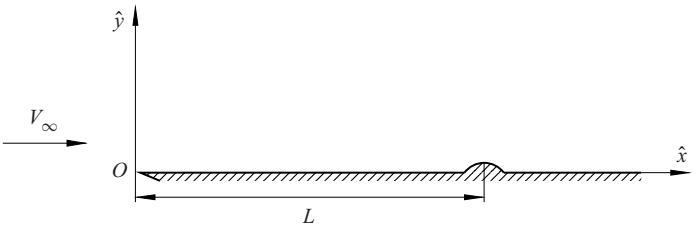

Figure 1. Flow layout.

with V_∞, p_∞, ρ_∞ and μ_∞ being the dimensional free-stream velocity, pressure, density and viscosity, respectively.

In the non-dimensional variables, the Navier–Stokes equations are written as

$$\rho\left(\frac{\partial u}{\partial t}+u\frac{\partial u}{\partial x}+v\frac{\partial u}{\partial y}\right)=-\frac{\partial p}{\partial x}+\frac{1}{Re}\left\{\frac{\partial}{\partial x}\left[\mu\left(\frac{4}{3}\frac{\partial u}{\partial x}-\frac{2}{3}\frac{\partial v}{\partial y}\right)\right]+\frac{\partial}{\partial y}\left[\mu\left(\frac{\partial u}{\partial y}+\frac{\partial v}{\partial x}\right)\right]\right\}, \tag{2.2a}$$

$$\rho\left(\frac{\partial v}{\partial t}+u\frac{\partial v}{\partial x}+v\frac{\partial v}{\partial y}\right)=-\frac{\partial p}{\partial y}+\frac{1}{Re}\left\{\frac{\partial}{\partial y}\left[\mu\left(\frac{4}{3}\frac{\partial v}{\partial y}-\frac{2}{3}\frac{\partial u}{\partial x}\right)\right]+\frac{\partial}{\partial x}\left[\mu\left(\frac{\partial u}{\partial y}+\frac{\partial v}{\partial x}\right)\right]\right\}, \tag{2.2b}$$

$$\rho\left(\frac{\partial h}{\partial t}+u\frac{\partial h}{\partial x}+v\frac{\partial h}{\partial y}\right)=\frac{\partial p}{\partial t}+u\frac{\partial p}{\partial x}+v\frac{\partial p}{\partial y}+\frac{1}{Re}\left\{\frac{1}{Pr}\left[\frac{\partial}{\partial x}\left(\mu\frac{\partial h}{\partial x}\right)+\frac{\partial}{\partial y}\left(\mu\frac{\partial h}{\partial y}\right)\right]+\mu\left(\frac{4}{3}\frac{\partial u}{\partial x}-\frac{2}{3}\frac{\partial v}{\partial y}\right)\frac{\partial u}{\partial x}+\mu\left(\frac{4}{3}\frac{\partial v}{\partial y}-\frac{2}{3}\frac{\partial u}{\partial x}\right)\frac{\partial v}{\partial y}+\mu\left(\frac{\partial u}{\partial y}+\frac{\partial v}{\partial x}\right)^2\right\}, \tag{2.2c}$$

$$\frac{\partial \rho}{\partial t}+\frac{\partial \rho u}{\partial x}+\frac{\partial \rho v}{\partial y}=0, \tag{2.2d}$$

$$h=\frac{1}{(\gamma-1)M_\infty^2}\frac{1}{\rho}+\frac{\gamma}{\gamma-1}\frac{p}{\rho}. \tag{2.2e}$$

Here, Pr is the Prandtl number and γ is the specific heat ratio; for air $Pr\approx 0.713$, $\gamma=7/5$. The Reynolds number Re is calculated as

$$Re=\frac{\rho_\infty V_\infty L}{\mu_\infty}. \tag{2.3}$$

In this study, we shall assume that Re is large, while the free-stream Mach number, $M_\infty=V_\infty/a_\infty$, remains finite. In fact, we shall restrict our attention to the subsonic flows where $M_\infty<1$.

3. Unperturbed flow

Our first task is to describe the steady unperturbed flow. At large values of the Reynolds number, the boundary-layer theory of Prandtl (1904) can be used for this purpose. According to this theory, the flow field should be divided into two regions: the inviscid

region occupying the majority of the flow and the thin boundary layer that forms on the surface of the plate. In the inviscid region, the flow remains unperturbed in the leading-order approximation with the fluid-dynamic functions preserving their values in the oncoming flow before the plate

$$u = 1, \quad v = 0, \quad p = 0, \quad \rho = 1, \quad h = \frac{1}{(\gamma - 1)M_\infty^2}. \tag{3.1a–e}$$

When dealing with the boundary layer we assume that

$$x = O(1), \quad Y = Re^{1/2}y = O(1), \quad Re \to \infty, \tag{3.2a–c}$$

and represent the corresponding solution of the Navier–Stokes equations (2.2) in the form

$$\left.\begin{aligned} u(t, x, y; Re) &= U_0(x, Y) + \cdots, \quad v(t, x, y; Re) = Re^{-1/2}V_0(x, Y) + \cdots, \\ \rho(t, x, y; Re) &= \rho_0(x, Y) + \cdots, \quad p(t, x, y; Re) = Re^{-1/2}P_0(x, Y) + \cdots, \\ h(t, x, y; Re) &= h_0(x, Y) + \cdots, \quad \mu(t, x, y; Re) = \mu_0(x, Y) + \cdots. \end{aligned}\right\} \tag{3.3}$$

Substitution of (3.3) into the Navier–Stokes equations (2.2) leads to classical boundary-layer equations for compressible flow. A detailed discussion of these equations together with corresponding boundary conditions may be found in § 1.10 in the book by Ruban (2018). We shall assume here that the plate surface is thermally isolated, in which case the boundary-layer equations admit a self-similar solution in the form

$$\left.\begin{aligned} U_0(x, Y) = \tilde{U}(\eta), \quad V_0(x, Y) = \frac{1}{\sqrt{x}}\tilde{V}(\eta), \quad \rho_0(x, Y) = \tilde{\rho}(\eta), \\ h_0(x, Y) = \tilde{h}(\eta), \quad \mu_0(x, Y) = \tilde{\mu}(\eta), \end{aligned}\right\} \tag{3.4}$$

where

$$\eta = \frac{Y}{\sqrt{x}}. \tag{3.5}$$

Functions $\tilde{U}, \tilde{V}, \tilde{h}$ and $\tilde{\rho}$ are to be found by solving the following set of ordinary differential equations:

$$-\frac{1}{2}\eta\tilde{\rho}\tilde{U}\frac{\mathrm{d}\tilde{U}}{\mathrm{d}\eta} + \tilde{\rho}\tilde{V}\frac{\mathrm{d}\tilde{U}}{\mathrm{d}\eta} = \frac{\mathrm{d}}{\mathrm{d}\eta}\left(\tilde{\mu}\frac{\mathrm{d}\tilde{U}}{\mathrm{d}\eta}\right), \tag{3.6a}$$

$$-\frac{1}{2}\eta\tilde{\rho}\tilde{U}\frac{\mathrm{d}\tilde{h}}{\mathrm{d}\eta} + \tilde{\rho}\tilde{V}\frac{\mathrm{d}\tilde{h}}{\mathrm{d}\eta} = \frac{1}{Pr}\frac{\mathrm{d}}{\mathrm{d}\eta}\left(\tilde{\mu}\frac{\mathrm{d}\tilde{h}}{\mathrm{d}\eta}\right) + \tilde{\mu}\left(\frac{\mathrm{d}\tilde{U}}{\mathrm{d}\eta}\right)^2, \tag{3.6b}$$

$$-\frac{1}{2}\eta\frac{d}{d\eta}(\tilde{\rho}\tilde{U}) + \frac{\mathrm{d}}{\mathrm{d}\eta}(\tilde{\rho}\tilde{V}) = 0, \tag{3.6c}$$

$$\tilde{h} = \frac{1}{(\gamma - 1)M_\infty^2}\frac{1}{\tilde{\rho}}, \tag{3.6d}$$

subject to the boundary conditions

$$\tilde{U} = 1, \quad \tilde{h} = \frac{1}{(\gamma - 1)M_\infty^2} \quad \text{at } \eta = \infty, \tag{3.6e}$$

$$\tilde{U} = \tilde{V} = 0, \quad \frac{\mathrm{d}\tilde{h}}{\mathrm{d}\eta} = 0, \quad \text{at } \eta = 0. \tag{3.6f}$$

To perform the receptivity analysis of the boundary layer, we need to know the behaviour of the solution to (3.6) near the plate surface ($\eta \to 0$) and at the outer edge of the boundary layer ($\eta \to \infty$). In view of (3.6*f*) the Taylor expansions of $\tilde{U}$ and $\tilde{h}$ near the plate surface may be written as

$$\tilde{U} = \lambda\eta + \cdots, \quad \tilde{h} = h_w + O(\eta^2), \quad \text{as } \eta \to 0, \tag{3.7}$$

where constants λ and h_w are found through a numerical solution of the boundary value problem (3.6).

To describe the behaviour of the solution near the outer edge of the boundary layer we use the procedure suggested in problem 2 in exercises 1 in Ruban (2018). We find that

$$\tilde{U} = 1 - \frac{C}{2(\eta - B)}\,\mathrm{e}^{-(\eta-B)^2/4} + \cdots, \quad \text{as } \eta \to \infty. \tag{3.8}$$

Constants C and B are found through numerical solution of (3.6) as a whole.

4. Entropy waves

The flow upstream of the leading edge of the plate and in the inviscid region above the plate is given in the leading-order approximation by (3.1*a–e*). We shall now perturb this flow

$$\left.\begin{gathered} u = 1 + \varepsilon u'(t,x,y), \quad v = \varepsilon v'(t,x,y), \quad \rho = 1 + \varepsilon\rho'(t,x,y), \\ p = \varepsilon p'(t,x,y), \quad h = \frac{1}{(\gamma-1)M_\infty^2} + \varepsilon h'(t,x,y), \end{gathered}\right\} \tag{4.1}$$

where ε is a small parameter representing the amplitude of the perturbations.

Substituting (4.1) into the Navier–Stokes equations (2.2) and working with the $O(\varepsilon)$ terms we arrive at the linearised Euler equations

$$\left.\begin{gathered} \frac{\partial u'}{\partial t} + \frac{\partial u'}{\partial x} = -\frac{\partial p'}{\partial x}, \\ \frac{\partial v'}{\partial t} + \frac{\partial v'}{\partial x} = -\frac{\partial p'}{\partial y}, \\ \frac{\partial h'}{\partial t} + \frac{\partial h'}{\partial x} = \frac{\partial p'}{\partial t} + \frac{\partial p'}{\partial x}, \\ \frac{\partial \rho'}{\partial t} + \frac{\partial \rho'}{\partial x} + \frac{\partial u'}{\partial x} + \frac{\partial v'}{\partial y} = 0, \\ h' = \frac{\gamma}{\gamma-1}p' - \frac{1}{(\gamma-1)M_\infty^2}\rho'. \end{gathered}\right\} \tag{4.2}$$

According to Kovasznay (1953), an arbitrary small perturbation to uniform compressible flow can be represented as a superposition of acoustic noise, vorticity waves and entropy waves. If the amplitude of these modes is small, then they may be considered independent of one another. As was already mentioned, the generation of the Tollmien–Schlichting waves by acoustic noise and by vorticity waves were studied by Ruban (1984) and Goldstein (1985) and by Duck *et al.* (1996), respectively. In this paper, we are concerned

with the entropy waves, where

$$u' = v' = p' = 0, \tag{4.3}$$

and (4.2) reduce to

$$\frac{\partial h'}{\partial t} + \frac{\partial h'}{\partial x} = 0, \tag{4.4a}$$

$$\frac{\partial \rho'}{\partial t} + \frac{\partial \rho'}{\partial x} = 0, \tag{4.4b}$$

$$h' = -\frac{1}{(\gamma - 1)M_\infty^2}\rho'. \tag{4.4c}$$

The general solutions to (4.4*a*), (4.4*b*) are written as

$$h' = f(x - t, y), \quad \rho' = g(x - t, y), \tag{4.5a,b}$$

which shows that the entropy waves propagate downstream with the mean free-stream velocity. We shall assume that the free-stream turbulence is uniform, in which case h' and ρ' can be represented as a superposition of the Fourier harmonics

$$h' = \sum_{i,j} h_{i,j} \exp\left(\mathrm{i}[\alpha_i(x - t) + \beta_j y]\right) + (\text{c.c.}),$$

$$\rho' = \sum_{i,j} \rho_{i,j} \exp\left(\mathrm{i}[\alpha_i(x - t) + \beta_j y]\right) + (\text{c.c.}), \tag{4.6a,b}$$

where the longitudinal and lateral wavenumbers, α_i and β_j, are real, and (c.c.) denotes the complex conjugate of the quantity in front of it. For efficient receptivity, only the harmonics that are in resonance with the Tollmien–Schlichting waves are important, namely, have an $O(Re^{1/4})$ frequency. Keeping this in mind, we introduce the 'fast' time and coordinates

$$\bar{t} = Re^{1/4}t, \quad \bar{x} = Re^{1/4}x, \quad \bar{y} = Re^{1/4}y, \tag{4.7a–c}$$

and consider a harmonic from (4.6*a*,*b*). We can express it in the form

$$h' = h_a \exp(\mathrm{i}\alpha\xi + \beta\bar{y}) + (\text{c.c.}), \quad \rho' = \rho_a \exp(\mathrm{i}\alpha\xi + \beta\bar{y}) + (\text{c.c.}), \tag{4.8a,b}$$

where

$$\xi = \bar{x} - \bar{t}. \tag{4.9}$$

It follows from (4.4*c*) that h_a and ρ_a are related to one another as

$$\rho_a = -(\gamma - 1)M_\infty^2 h_a. \tag{4.10}$$

Through appropriate adjustment of the amplitude parameter ε in (4.1) we can always make $\rho_a = 1$, and then we will have

$$h' = -\frac{1}{(\gamma - 1)M_\infty^2} \exp(\mathrm{i}\alpha\xi + \beta\bar{y}) + (\text{c.c.}), \quad \rho' = \exp(\mathrm{i}\alpha\xi + \beta\bar{y}) + (\text{c.c.}). \tag{4.11a,b}$$

5. Transition layer

Since the entropy waves do not produce the pressure perturbations, they cannot penetrate the boundary layer. To smooth out the corresponding jump in the entropy and density one needs to introduce a transition layer. The situation is similar to the one encountered in the case of vorticity waves; see Gulyaev *et al.* (1989).

We seek the solution in the transition layer in the form

$$\left.\begin{aligned} u &= U_0(x, Y) + o(\varepsilon), \\ v &= Re^{-1/2} V_0(x, Y) + \sigma v_1(\xi, \bar{Y}; x) + \cdots, \\ p &= Re^{-1/2} P_0(x, Y) + o(\varepsilon), \\ h &= h_0(x, Y) + \varepsilon h_1(\xi, \bar{Y}; x) + \cdots, \\ \rho &= \rho_0(x, Y) + \varepsilon \rho_1(\xi, \bar{Y}; x) + \cdots, \\ \mu &= \mu_0(x, Y) + \varepsilon \mu_1(\xi, \bar{Y}; x) + \cdots. \end{aligned}\right\} \tag{5.1}$$

Here, it is assumed that the perturbations of the longitudinal velocity u and of the pressure p are small compared with ε, and can be disregarded. The perturbations of the enthalpy h and density ρ are of the same order, $O(\varepsilon)$, as those outside the boundary layer. The parameter σ in the asymptotic expansion of the lateral velocity v is not known in advance but we expect to find it when analysing the continuity equation (2.2*b*). The perturbation terms in (5.1) are assumed to be functions of the phase variable ξ and a new transverse coordinate $\bar{Y}$. We will see that they also depend on x as a parameter. Using (4.7*a–c*) in (4.9) we can express the phase variable as $\xi = Re^{1/4}(x - t)$. The transverse coordinate $\bar{Y}$ is defined by the equation

$$y = Re^{-1/2}\left[\Delta(Re)\sqrt{x} + B\sqrt{x} + \delta(Re)\bar{Y}\right]. \tag{5.2}$$

Here, $\Delta(Re)$ is assumed large, and $\delta(Re)$ small, that is

$$\Delta(Re) \to \infty, \quad \delta(Re) \to 0 \quad \text{as } Re \to \infty. \tag{5.3}$$

We now need to substitute (5.1) into the Navier–Stokes equations. Since this procedure is rather delicate, we shall give here some details of our calculations. We start with the continuity equation (2.2*b*). We have

$$\frac{\partial \rho}{\partial t} = -\varepsilon Re^{1/4} \frac{\partial \rho_1}{\partial \xi} + \cdots, \tag{5.4}$$

$$u\frac{\partial \rho}{\partial x} = U_0 \frac{\partial \rho_0}{\partial x} + \varepsilon Re^{1/4} U_0 \frac{\partial \rho_1}{\partial \xi} - \frac{\varepsilon \Delta}{\delta} \frac{1}{2\sqrt{x}} \frac{\partial \rho_1}{\partial \bar{Y}} + \cdots, \tag{5.5}$$

$$\rho\frac{\partial u}{\partial x} = \rho_0 \frac{\partial U_0}{\partial x} + \varepsilon \frac{\partial U_0}{\partial x} \rho_1 + \cdots, \tag{5.6}$$

$$v\frac{\partial \rho}{\partial y} = V_0 \frac{\partial \rho_0}{\partial Y} + \frac{\varepsilon}{\delta} V_0 \frac{\partial \rho_1}{\partial \bar{Y}} + \sigma Re^{1/2} \frac{\partial \rho_0}{\partial Y} v_1 + \cdots, \tag{5.7}$$

$$\rho\frac{\partial v}{\partial y} = \rho_0 \frac{\partial V_0}{\partial Y} + \frac{\sigma Re^{1/2}}{\delta} \rho_0 \frac{\partial v_1}{\partial \bar{Y}} + \varepsilon \frac{\partial V_0}{\partial Y} \rho_1 + \cdots. \tag{5.8}$$

We substitute these into (2.2*b*) and work with the perturbations terms

$$-\varepsilon Re^{1/4}(1-U_0)\frac{\partial \rho_1}{\partial \xi} - \underbrace{\frac{\varepsilon \Delta}{\delta}\frac{1}{2\sqrt{x}}\frac{\partial \rho_1}{\partial \bar{Y}}}_{1} + \underbrace{\varepsilon \frac{\partial U_0}{\partial x}\rho_1}_{2}$$
$$+ \underbrace{\frac{\varepsilon}{\delta}V_0\frac{\partial \rho_1}{\partial \bar{Y}}}_{3} + \underbrace{\sigma Re^{1/2}\frac{\partial \rho_0}{\partial Y}v_1}_{4} + \underbrace{\frac{\sigma Re^{1/2}}{\delta}\rho_0\frac{\partial v_1}{\partial \bar{Y}}}_{5} + \underbrace{\varepsilon \frac{\partial V_0}{\partial Y}\rho_1}_{6} = 0. \tag{5.9}$$

Keeping in mind that Δ is large and δ is small, we can see that terms 2, 3 and 6 are small compared with term 1. We can also see that term 4 is small compared with term 5. This simplifies the continuity equation to

$$-\varepsilon Re^{1/4}(1-U_0)\frac{\partial \rho_1}{\partial \xi} - \frac{\varepsilon \Delta}{\delta}\frac{1}{2\sqrt{x}}\frac{\partial \rho_1}{\partial \bar{Y}} + \frac{\sigma Re^{1/2}}{\delta}\rho_0\frac{\partial v_1}{\partial \bar{Y}} = 0. \tag{5.10}$$

Similarly, the energy equation (2.2*c*) yields

$$-\varepsilon Re^{1/4}(1-U_0)\frac{\partial h_1}{\partial \xi} - \frac{\varepsilon \Delta}{\delta}\frac{1}{2\sqrt{x}}\frac{\partial h_1}{\partial \bar{Y}} + \sigma Re^{1/2}\frac{\partial h_0}{\partial Y}v_1 = \frac{\varepsilon}{\delta^2}\frac{\mu_0}{\rho_0}\frac{\partial^2 h_1}{\partial \bar{Y}^2}. \tag{5.11}$$

The boundary conditions for equations (5.10) and (5.11) are written as

$$h_1 = -\frac{e^{i\alpha\xi}}{(\gamma-1)M_\infty^2} + (\text{c.c.}) \quad \text{at } \bar{Y} = \infty, \tag{5.12a}$$
$$h_1 = v_1 = 0 \quad \text{at } \bar{Y} = -\infty. \tag{5.12b}$$

Condition (5.12*a*) is obtained by matching with the solution (4.11*a*,*b*) outside the boundary layer. Condition (5.12*b*) signifies that the perturbations do not penetrate the boundary layer.

To progress further, we need to know the behaviour of $1-U_0$ in the transition layer where $\bar{Y}$ is finite. Using (5.2) in (3.8) we find that

$$1-U_0 = \frac{C}{2\Delta}e^{-\Delta^2/4}e^{-\Delta\delta\bar{Y}/2\sqrt{x}}. \tag{5.13}$$

Considering (5.10) and (5.11), we notice that if the coefficients in these equations were constant, then the periodic in ξ solution would be a superposition of the exponential functions, $\sum A_i e^{\lambda_i \bar{Y}}$. This would make it impossible to satisfy boundary conditions (5.12). In order to prevent this, we set

$$\Delta\delta = 2, \tag{5.14}$$

which turns (5.13) into

$$1-U_0 = \frac{C}{2\Delta}e^{-\Delta^2/4}e^{-\bar{Y}/\sqrt{x}}. \tag{5.15}$$

It is easily seen that, with (5.14), the second term on the left-hand side of (5.11) appears to be the same order as the term on the right-hand side. We know that for The boundary (5.11) to have the required properties, it should retain the first term on left-hand side as

this is the only term with a non-constant coefficient (5.15). To satisfy this requirement, we set

$$Re^{1/4}\frac{C}{2\Delta}\,\mathrm{e}^{-\Delta^2/4}=\frac{1}{\delta^2}. \tag{5.16}$$

With (5.14) and (5.16), (5.10) and (5.11) assume the form

$$-\frac{\varepsilon}{\delta^2}\mathrm{e}^{-\bar{Y}/\sqrt{x}}\frac{\partial\rho_1}{\partial\xi}-\frac{\varepsilon\Delta}{\delta}\frac{1}{2\sqrt{x}}\frac{\partial\rho_1}{\partial\bar{Y}}+\frac{\sigma Re^{1/2}}{\delta}\rho_0\frac{\partial v_1}{\partial\bar{Y}}=0, \tag{5.17}$$

$$-\frac{\varepsilon}{\delta^2}\mathrm{e}^{-\bar{Y}/\sqrt{x}}\frac{\partial h_1}{\partial\xi}-\frac{\varepsilon\Delta}{\delta}\frac{1}{2\sqrt{x}}\frac{\partial h_1}{\partial\bar{Y}}+\sigma Re^{1/2}\frac{\partial h_0}{\partial Y}v_1=\frac{\varepsilon}{\delta^2}\frac{\mu_0}{\rho_0}\frac{\partial^2 h_1}{\partial\bar{Y}^2}. \tag{5.18}$$

Parameters Δ and δ are defined by (5.14) and (5.16) uniquely, and it may be shown that they satisfy conditions (5.3). Now we need to determine parameter σ. If we assume that

$$\frac{\sigma Re^{1/2}}{\delta}\gg\frac{\varepsilon}{\delta^2}, \tag{5.19}$$

then the third term in the continuity equation (5.17) would be dominant, and we would have

$$\frac{\partial v_1}{\partial\bar{Y}}=0. \tag{5.20}$$

However, integration of (5.20) with condition on v_1 in (5.12*b*) leads to a conclusion that v_1 is identically zero in the transition layer. This means that assumption (5.19) overestimates σ and should be rejected.

If, on the other hand

$$\frac{\sigma Re^{1/2}}{\delta}=\frac{\varepsilon}{\delta^2}, \tag{5.21}$$

or

$$\frac{\sigma Re^{1/2}}{\delta}\ll\frac{\varepsilon}{\delta^2}, \tag{5.22}$$

then the third term on the left-hand side of the energy equation (5.18) can be disregarded, and we can conclude that h_1 satisfies the equation

$$-\mathrm{e}^{-\bar{Y}/\sqrt{x}}\frac{\partial h_1}{\partial\xi}-\frac{1}{\sqrt{x}}\frac{\partial h_1}{\partial\bar{Y}}=\frac{\partial^2 h_1}{\partial\bar{Y}^2}. \tag{5.23}$$

Here, it is taken into account that the transition layer lies at the outer edge of the boundary layer, where $\mu_0=\rho_0=1$.

We seek the solution to (5.23) in the form

$$h_1(x,\xi,\bar{Y})=\mathrm{e}^{\mathrm{i}\alpha\xi}\breve{h}_1(x,\bar{Y})+(\text{c.c.}). \tag{5.24}$$

Substitution of (5.24) into (5.23) and into the boundary conditions for h_1 in (5.12) yields the following boundary-value problem for $\breve{h}_1$:

$$\frac{\partial^2\breve{h}_1}{\partial\bar{Y}^2}+\frac{1}{\sqrt{x}}\frac{\partial\breve{h}_1}{\partial\bar{Y}}+\mathrm{i}\alpha\mathrm{e}^{-\bar{Y}/\sqrt{x}}\breve{h}_1=0, \tag{5.25a}$$

$$\breve{h}_1\Big|_{\bar{Y}=\infty}=-\frac{1}{(\gamma-1)M_\infty^2},\quad \breve{h}_1\Big|_{\bar{Y}=-\infty}=0. \tag{5.25b}$$

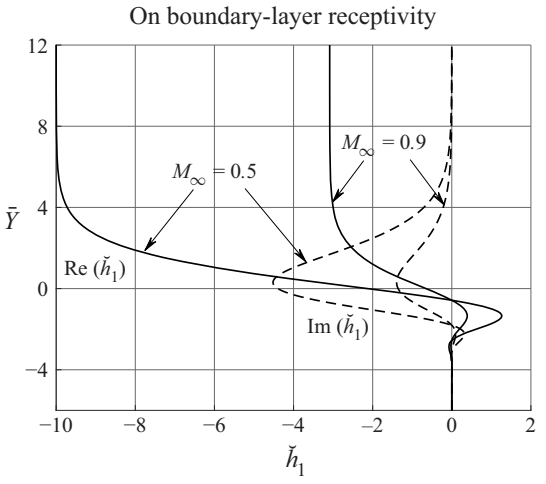

Figure 2. The real (bold line) and imaginary (dashed line) parts of function $\check{h}_1$ calculated for $x = 1$, $\alpha = 1$ and two values of the Mach number, $M_\infty = 0.5$ and 0.9.

The change of variables

$$\check{h}_1 = zw(z), \quad z = 2(i\alpha x)^{1/2}\mathrm{e}^{-\bar{Y}/(2\sqrt{x})} \tag{5.26}$$

turns (5.25*a*) into the Bessel equation

$$z^2\frac{\mathrm{d}^2w}{\mathrm{d}z^2} + z\frac{\mathrm{d}w}{\mathrm{d}z} + \left(z^2 - 1\right)w = 0. \tag{5.27a}$$

The boundary conditions (5.25*b*) are written in these variables as

$$w = -\frac{1}{(\gamma-1)M_\infty^2}z^{-1} + \cdots \quad \text{as } z \to 0, \tag{5.27b}$$

$$w \to 0 \quad \text{as } z \to \infty. \tag{5.27c}$$

In (5.27*c*), z should tend to infinity along the ray where $\arg z = \pi/4$.

The solution of the boundary-value problem (5.27) is given by

$$w(z) = -\frac{\pi\mathrm{i}}{2(\gamma-1)M_\infty^2}H_1^{(1)}(z), \tag{5.28}$$

where $H_1^{(1)}(z)$ is the Hankel function of the first kind. It remains to substitute (5.28) back into (5.26) and then into (5.24), and we can conclude that in the transition layer

$$h_1 = -\frac{\pi i}{2(\gamma-1)M_\infty^2}\mathrm{e}^{\mathrm{i}\alpha\xi}zH_1^{(1)}(z). \tag{5.29}$$

The graphic illustration of this solution is presented in figure 2.

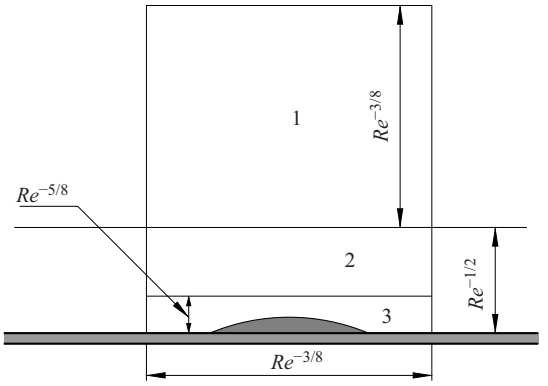

Figure 3. The flow in the vicinity of the wall roughness.

With known h_1 we can use the state (2.2*c*) to find the density perturbations in the transition layer. We have

$$\rho_1 = -(\gamma - 1)M_\infty^2 h_1 = \frac{\pi \mathrm{i}}{2}\,\mathrm{e}^{\mathrm{i}\alpha\xi} z H_1^{(1)}(z) + (\text{c.c.}). \tag{5.30}$$

Now we can return to the continuity equation (5.17). To avoid a degeneration in this equation, we need to choose σ according to (5.21), that is

$$\sigma = Re^{-1/2}\frac{\varepsilon}{\delta}, \tag{5.31}$$

and then the continuity equation assumes the form

$$\frac{\partial v_1}{\partial \bar{Y}} = \mathrm{e}^{-\bar{Y}/\sqrt{x}}\frac{\partial \rho_1}{\partial \xi} + \frac{1}{\sqrt{x}}\frac{\partial \rho_1}{\partial \bar{Y}}. \tag{5.32}$$

It has to be integrated with the disturbance attenuation condition (5.12*b*)

$$v_1 = 0 \quad \text{at } \bar{Y} = -\infty. \tag{5.33}$$

We shall leave this task for others to perform.

6. Triple-deck region

The generation of Tollmien–Schlichting waves takes place as a result of the interaction of the entropy waves with steady flow perturbations caused by a wall roughness. We have chosen the frequency of the entropy waves to be $\omega = O(Re^{1/4})$. This is to satisfy the resonance condition. The second resonance condition requires the roughness size Δx to be comparable to the wavelength of the Tollmien–Schlichting wave, that is $\Delta x = O(Re^{-3/8})$. It is well known that the flow past a roughness of this size is described by the triple-deck theory. According to this theory, when analysing the flow in the vicinity of the roughness one has to consider three regions: the viscous sublayer (region 3 in figure 3), the main part of the boundary layer (region 2) and in the upper region 1 that lies in the inviscid flow outside the boundary layer.

In this section our task is to derive the equations that describe the flow in the three layers. When performing this task we shall assume the roughness shape can be represented by the equation

$$y = Re^{-5/8} F\left(\frac{x-1}{Re^{-3/8}}\right). \tag{6.1}$$

6.1. *Upper tier*

In order to predict the form of asymptotic expansions of fluid-dynamic functions in the upper tier of the triple-deck region, we return to the solution (4.11*a*,*b*) for the inviscid flow upstream of the roughness. Substituting (4.7*a–c*) into (4.9) and then into (4.11*a*,*b*), we see that near the roughness, the solution for the entropy wave may be written in the form

$$\left.\begin{gathered} u = 1 + \varepsilon \cdot 0, \quad v = \varepsilon \cdot 0, \quad p = \varepsilon \cdot 0, \\ \rho = 1 + \varepsilon \rho_0'(\bar{t}), \quad h = \frac{1}{(\gamma-1)M_\infty^2} + \varepsilon h_0'(\bar{t}), \end{gathered}\right\} \tag{6.2}$$

where

$$\rho_0'(\bar{t}) = \rho_\alpha \mathrm{e}^{\mathrm{i}\omega\bar{t}} + (\text{c.c.}), \quad h_0'(\bar{t}) = h_\alpha \mathrm{e}^{\mathrm{i}\omega\bar{t}} + (\text{c.c.}). \tag{6.3a,b}$$

The frequency of oscillations ω coincides with the wavenumber α of the entropy wave, and the amplitude is given by

$$\rho_\alpha = \mathrm{e}^{-\mathrm{i}\alpha\bar{x}_0}, \quad h_\alpha = -\frac{\mathrm{e}^{-\mathrm{i}\alpha\bar{x}_0}}{(\gamma-1)M_\infty^2}, \tag{6.4a,b}$$

where $\bar{x}_0$ denoting the value of $\bar{x}$ at the position of the roughness.

Keeping further in mind that the wall roughness (6.1) produces $O(Re^{-1/4})$ steady perturbations in the flow, we represent the fluid-dynamic functions in the upper tier in the form

$$\left.\begin{aligned} u &= 1 + Re^{-1/4}u_1^*(x_*, y_*) + \varepsilon Re^{-1/4}u_2^*(\bar{t}, x_*, y_*) + \cdots, \\ v &= Re^{-1/4}v_1^*(x_*, y_*) + \varepsilon Re^{-1/4}v_2^*(\bar{t}, x_*, y_*) + \cdots, \\ p &= Re^{-1/4}p_1^*(x_*, y_*) + \varepsilon Re^{-1/4}p_2^*(\bar{t}, x_*, y_*) + \cdots, \\ \rho &= 1 + \varepsilon\rho_0'(\bar{t}) + Re^{-1/4}\rho_1^*(x_*, y_*) + \varepsilon Re^{-1/4}\rho_2^*(\bar{t}, x_*, y_*) + \cdots, \\ h &= \frac{1}{(\gamma-1)M_\infty^2} + \varepsilon h_0'(\bar{t}) + Re^{-1/4}h_1^*(x_*, y_*) + \varepsilon Re^{-1/4}h_2^*(\bar{t}, x_*, y_*) + \cdots, \end{aligned}\right\} \tag{6.5}$$

with the independent variables being

$$\bar{t} = \frac{t}{Re^{-1/4}}, \quad x_* = \frac{x-1}{Re^{-3/8}}, \quad y_* = \frac{y}{Re^{-3/8}}. \tag{6.6a–c}$$

The $O(\varepsilon Re^{-1/4})$ terms in (6.5) represent the perturbations produced by the interaction of the unsteady perturbations in the entropy wave with the steady caused by the wall roughness.

The equations for the $O(Re^{-1/4})$ and $O(\varepsilon Re^{-1/4})$ terms are obtained by substituting (6.5), (6.6*a–c*) into the Navier–Stokes equations (2.2). The perturbations produced by the wall roughness are governed by the linearised Euler equations

$$\left.\begin{gathered} \frac{\partial u_1^*}{\partial x_*} = -\frac{\partial p_1^*}{\partial x_*}, \quad \frac{\partial v_1^*}{\partial x_*} = -\frac{\partial p_1^*}{\partial y_*}, \quad \frac{\partial h_1^*}{\partial x_*} = \frac{\partial p_1^*}{\partial x_*}, \\ \frac{\partial u_1^*}{\partial x_*} + \frac{\partial \rho_1^*}{\partial x_*} + \frac{\partial v_1^*}{\partial y_*} = 0, \quad h_1^* = \frac{\gamma}{\gamma-1}p_1^* - \frac{1}{(\gamma-1)M_\infty^2}\rho_1^*. \end{gathered}\right\} \tag{6.7}$$

These equations were encountered on numerous occasions before in the context of the triple-deck theory; see § 4.2.3 in Ruban (2018). They may be reduced, by means of

elimination, to a single equation for the pressure p_1^*

$$(1-M_\infty^2)\frac{\partial p_1^*}{\partial x_*^2}+\frac{\partial p_1^*}{\partial y_*^2}=0. \tag{6.8}$$

With known p_1^* the enthalpy h_1^*, longitudinal velocity u_1^* and density ρ_1^* are calculated as

$$h_1^*=p_1^*,\quad u_1^*=-p_1^*,\quad \rho_1^*=M_\infty^2 p_1^*. \tag{6.9a–c}$$

The equations for the $O(\varepsilon Re^{-1/4})$ terms are found to be

$$\frac{\partial u_2^*}{\partial x_*}+\frac{\partial p_2^*}{\partial x_*}=-\rho_0'(\bar t)\frac{\partial u_1^*}{\partial x_*}, \tag{6.10a}$$

$$\frac{\partial v_2^*}{\partial x_*}+\frac{\partial p_2^*}{\partial y_*}=-\rho_0'(\bar t)\frac{\partial v_1^*}{\partial x_*}, \tag{6.10b}$$

$$\frac{\partial h_2^*}{\partial x_*}-\frac{\partial p_2^*}{\partial x_*}=-\rho_0'(\bar t)\frac{\partial h_1^*}{\partial x_*}, \tag{6.10c}$$

$$\frac{\partial u_2^*}{\partial x_*}+\frac{\partial \rho_2^*}{\partial x_*}+\frac{\partial v_2^*}{\partial y_*}=-\rho_0'(\bar t)\left(\frac{\partial u_1^*}{\partial x_*}+\frac{\partial v_1^*}{\partial y_*}\right), \tag{6.10d}$$

$$h_2^*=\frac{\gamma}{\gamma-1}p_2^*-\frac{1}{(\gamma-1)M_\infty^2}\rho_2^*+\frac{2-\gamma}{\gamma-1}\rho_0'(\bar t)p_1^*. \tag{6.10e}$$

Performing the elimination routine again we find that the pressure p_2^* satisfies the following equation:

$$(1-M_\infty^2)\frac{\partial^2 p_2^*}{\partial x_*^2}+\frac{\partial^2 p_2^*}{\partial y_*^2}=\rho_0'(\bar t)M_\infty^2\frac{\partial^2 p_1^*}{\partial x_*^2}. \tag{6.11}$$

Before formulating the boundary conditions for (6.8) and (6.11) we need to consider the lower and middle tiers in the triple-deck structure (see figure 3).

6.2. *Lower tier*

Since the pressure does not change across the boundary layer, its asymptotic representation in the lower tier should be the same as in the upper tier; see the expansion for p in (6.5). Correspondingly, we shall seek the solution of the Navier–Stokes equations (2.2) in the lower tier in the form

$$\left.\begin{aligned} u&=Re^{-1/8}U_1^*(x_*,Y_*)+\varepsilon Re^{-1/8}U_2^*(\bar t,x_*,Y_*)+\cdots,\\ v&=Re^{-3/8}V_1^*(x_*,Y_*)+\varepsilon Re^{-3/8}V_2^*(\bar t,x_*,Y_*)+\cdots,\\ p&=Re^{-1/4}P_1^*(x_*,Y_*)+\varepsilon Re^{-1/4}P_2^*(\bar t,x_*,Y_*)+\cdots,\\ \rho&=\rho_w+\cdots,\quad h=h_w+\cdots,\quad \mu=\mu_w+\cdots. \end{aligned}\right\} \tag{6.12}$$

Here, the scaled time $\bar t$ and longitudinal coordinate x_* are the same (6.6a–c) as in the upper tier, while the lateral coordinate Y_* is introduced as

$$Y_*=\frac{y}{Re^{-5/8}}. \tag{6.13}$$

Since the flow in the lower tier is slow, it may be treated as incompressible with the density, enthalpy and viscosity coefficient being constant. We denote their values as ρ_w, h_w

and μ_w, respectively. These are obtained from the solution of the boundary-layer equations at the position of the roughness

$$\rho_w = \rho_0(1,0), \quad h_w = h_0(1,0), \quad \mu_w = \mu_0(1,0). \tag{6.14a–c}$$

Substitution of (6.12) into the Navier–Stokes equations (2.2) yields in the leading-order approximation

$$\rho_w \left(U_1^* \frac{\partial U_1^*}{\partial x_*} + V_1^* \frac{\partial U_1^*}{\partial Y_*} \right) = -\frac{\partial P_1^*}{\partial x_*} + \mu_w \frac{\partial^2 U_1^*}{\partial Y_*^2}, \tag{6.15a}$$

$$\frac{\partial P_1^*}{\partial Y_*} = 0, \tag{6.15b}$$

$$\frac{\partial U_1^*}{\partial x_*} + \frac{\partial V_1^*}{\partial Y_*} = 0. \tag{6.15c}$$

These are conventional incompressible steady flow boundary-layer equations. They have to be solved with the no-slip conditions on the surface of the roughness (6.1)

$$U_1^* = V_1^* = 0 \quad \text{at } Y_* = F(x_*), \tag{6.16}$$

and the following condition of matching with the solution in the boundary layer upstream of the roughness:

$$U_1^* = \lambda Y_* \quad \text{at } x_* = -\infty, \tag{6.17}$$

where λ is dimensionless skin friction given by

$$\lambda = \left. \frac{\partial U_0}{\partial Y} \right|_{x=1,\, Y=0}. \tag{6.18}$$

It may be shown (see § 2.2.4 in Ruban 2018) that the solution to (6.15) satisfying condition (6.17) exhibits the following behaviour at the outer edge of the lower tier:

$$U_1^* = \lambda Y_* + A_1^*(x_*) + \cdots, \quad V_1^* = -\frac{\mathrm{d}A_1^*}{\mathrm{d}x_*} Y_* + \cdots \quad \text{as } Y_* \to \infty, \tag{6.19}$$

where $A_1^*(x_*)$ is termed the displacement function.

Now, turning to the second-order terms in (6.12), we have to consider the equations

$$\rho_w \left(\frac{\partial U_2^*}{\partial \bar{t}} + U_1^* \frac{\partial U_2^*}{\partial x_*} + U_2^* \frac{\partial U_1^*}{\partial x_*} + V_1^* \frac{\partial U_2^*}{\partial Y_*} + V_2^* \frac{\partial U_1^*}{\partial Y_*} \right) = -\frac{\partial P_2^*}{\partial x_*} + \mu_w \frac{\partial^2 U_2^*}{\partial Y_*^2}, \tag{6.20a}$$

$$\frac{\partial P_2^*}{\partial Y_*} = 0, \tag{6.20b}$$

$$\frac{\partial U_2^*}{\partial x_*} + \frac{\partial V_2^*}{\partial Y_*} = 0. \tag{6.20c}$$

They have to be solved subject of the no-slip conditions on the surface of the roughness

$$U_2^* = V_2^* = 0 \quad \text{at } Y_* = F(x_*), \tag{6.21}$$

and the matching condition with the solution in the boundary layer upstream of the roughness

$$U_2^* \to 0 \quad \text{as } x_* \to -\infty. \tag{6.22}$$

Again, it may be shown that at the outer edge of the lower tier

$$U_2^* = A_2^*(\bar{t}, x_*) + \cdots, \quad V_2^* = -\frac{\partial A_2^*}{\partial x_*} Y_* + \cdots \quad \text{as } Y_* \to \infty. \tag{6.23}$$

6.3. *Middle tier*

Region 2, the middle tier (see figure 3), represents a continuation of the conventional boundary layer into the triple-deck region. The thickness of region 2 is estimated as $y \sim Re^{-1/2}$. Consequently, the asymptotic analysis of the Navier–Stokes equations (2.2) in region 2 has to be performed based on the limit

$$\bar{t} = \frac{t}{Re^{-1/4}}, \quad x_* = \frac{x-1}{Re^{-3/8}} = O(1), \quad Y = \frac{y}{Re^{-1/2}} = O(1), \quad Re \to \infty. \quad (6.24a\text{–}d)$$

The form of the asymptotic expansions of the fluid-dynamic functions in region 2 may be predicted by analysing the solution in the overlap region that lies between regions 3 and 2. Let us examine the velocity components. In region 3, they are represented in the form of asymptotic expansions (6.12). At the outer edge of region 3, the coefficients in these expansions behave as described by (6.19) and (6.23). If we substitute (6.19), (6.23) into (6.12) and express the resulting equations in terms of variables of region 2, that is, perform the substitution $Y_* = Re^{1/8}Y$, then we will find that at the 'bottom' of region 2

$$\left.\begin{aligned} u &= \lambda Y + Re^{-1/8}A_1^*(x_*) + \varepsilon Re^{-1/8}A_2^*(\bar{t}, x_*) + \cdots, \\ v &= Re^{-1/4}\left(-\frac{\mathrm{d}A_1^*}{\mathrm{d}x_*}Y\right) + \varepsilon Re^{-1/4}\left(-\frac{\partial A_2^*}{\partial x_*}Y\right) + \cdots. \end{aligned}\right\} \quad (6.25)$$

This suggests that the solution in region 2 should be sought in the form

$$\left.\begin{aligned} u &= U_{00}(Y) + Re^{-1/8}\tilde{U}_1(x_*, Y) + \varepsilon Re^{-1/8}\tilde{U}_2(\bar{t}, x_*, Y) + \cdots, \\ v &= Re^{-1/4}\tilde{V}_1(x_*, Y) + \varepsilon Re^{-1/4}\tilde{V}_2(\bar{t}, x_*, Y) + \cdots. \end{aligned}\right\} \quad (6.26)$$

The leading-order term $U_{00}(Y)$ in the expansion for u coincides with the velocity profile in the boundary layer immediately before the triple-deck region. According to (3.7)

$$U_{00} = \lambda Y + \cdots \quad \text{as } Y \to 0. \quad (6.27)$$

It further follows from (6.25) that the perturbation terms $\tilde{U}_1(x_*, Y)$, $\tilde{U}_2(\bar{t}, x_*, Y)$, $\tilde{V}_1(x_*, Y)$ and $\tilde{V}_2(\bar{t}, x_*, Y)$ in (6.26) should exhibit the following behaviour at the 'bottom' of region 2:

$$\tilde{U}_1 = A_1^*(x_*) + \cdots, \quad \tilde{V}_1 = -\frac{\mathrm{d}A_1^*}{\mathrm{d}x_*}Y + \cdots \quad \text{as } Y \to 0, \quad (6.28)$$

and

$$\tilde{U}_2 = A_2^*(\bar{t}, x_*) + \cdots, \quad \tilde{V}_2 = -\frac{\partial A_2^*}{\partial x_*}Y + \cdots \quad \text{as } Y \to 0. \quad (6.29)$$

By analogy with the longitudinal velocity component u in (6.26), we shall seek the enthalpy h, the density ρ and the viscosity μ in region 2 in the form of the asymptotic expansions

$$\left.\begin{aligned} h &= h_{00}(Y) + Re^{-1/8}\tilde{h}_1(x_*, Y) + \varepsilon Re^{-1/8}\tilde{h}_2(\bar{t}, x_*, Y) + \cdots, \\ \rho &= \rho_{00}(Y) + Re^{-1/8}\tilde{\rho}_1(x_*, Y) + \varepsilon Re^{-1/8}\tilde{\rho}_2(\bar{t}, x_*, Y) + \cdots, \\ \mu &= \mu_{00}(Y) + Re^{-1/8}\tilde{\mu}_1(x_*, Y) + \varepsilon Re^{-1/8}\tilde{\mu}_2(\bar{t}, x_*, Y) + \cdots. \end{aligned}\right\} \quad (6.30)$$

Finally, we expect the pressure p to remain unchanged across the boundary layer. Consequently, the asymptotic representation of p in region 2 should have the same form

$$p = Re^{-1/4}\tilde{P}_1(x_*, Y) + \varepsilon Re^{-1/4}\tilde{P}_2(\bar{t}, x_*, Y) + \cdots \quad (6.31)$$

as that in region 3; see (6.12).

The substitution of (6.26), (6.30) and (6.31) into the Navier–Stokes equations (2.2) results in

$$\left.\begin{gathered} U_{00}(Y)\,\frac{\partial \tilde{U}_1}{\partial x_*} + \tilde{V}_1 \frac{\mathrm{d}U_{00}}{\mathrm{d}Y} = 0, \\ \frac{\partial \tilde{P}_1}{\partial Y} = 0, \\ U_{00}(Y)\,\frac{\partial \tilde{h}_1}{\partial x_*} + \tilde{V}_1 \frac{\mathrm{d}h_{00}}{\mathrm{d}Y} = 0, \\ \rho_{00}(Y)\frac{\partial \tilde{U}_1}{\partial x_*} + U_{00}(Y)\frac{\partial \tilde{\rho}_1}{\partial x_*} + \rho_{00}(Y)\frac{\partial \tilde{V}_1}{\partial Y} + \tilde{V}_1 \frac{\mathrm{d}\rho_{00}}{\mathrm{d}Y} = 0, \\ h_{00} = \frac{1}{(\gamma-1)M_\infty^2}\,\frac{1}{\rho_{00}}, \quad \tilde{h}_1 = -\frac{1}{(\gamma-1)M_\infty^2}\,\frac{\tilde{\rho}_1}{\rho_{00}^2}. \end{gathered}\right\} \tag{6.32}$$

The solution to (6.32) satisfying boundary conditions (6.28) is

$$\tilde{U}_1 = \frac{1}{\lambda} A_1^*(x_*) U_{00}'(Y), \quad \tilde{V}_1 = -\frac{1}{\lambda}\frac{\mathrm{d}A_1^*}{\mathrm{d}x_*} U_{00}(Y). \tag{6.33a,b}$$

The unsteady perturbation terms are analysed in the same way, leading to a conclusion that in the middle tier

$$\tilde{U}_2 = \frac{1}{\lambda} A_2^*(\bar{t}, x_*) U_{00}'(Y), \quad \tilde{V}_2 = -\frac{1}{\lambda}\frac{\partial A_2^*}{\partial x_*} U_{00}(Y). \tag{6.34a,b}$$

7. Viscous–inviscid interaction problem

We are now ready to formulate the boundary conditions for (6.8) and (6.11) in the upper tier. For this purpose we shall perform the matching of the streamline slope angle ϑ in regions 2 and 1. Using (6.26) we can calculate ϑ in region 2 (the middle tier) as

$$\vartheta = \arctan\frac{v}{u} = Re^{-1/4}\frac{\tilde{V}_1}{U_{00}} + \varepsilon Re^{-1/4}\frac{\tilde{V}_2}{U_{00}} + \cdots. \tag{7.1}$$

It then follows from (6.33*a*,*b*), (6.34*a*,*b*) that

$$\vartheta = Re^{-1/4}\left(-\frac{1}{\lambda}\frac{\mathrm{d}A_1^*}{\mathrm{d}x_*}\right) + \varepsilon Re^{-1/4}\left(-\frac{1}{\lambda}\frac{\partial A_2^*}{\partial x_*}\right) + \cdots. \tag{7.2}$$

To calculate ϑ in the upper tier, we have to use the asymptotic expansions of u and v given by (6.5). We have

$$\vartheta = \arctan\frac{v}{u} = Re^{-1/4} v_1^*(x_*, y_*) + \varepsilon Re^{-1/4} v_2^*(\bar{t}, x_*, y_*) + \cdots. \tag{7.3}$$

We now need to set $y_* \to 0$ in (7.3) and compare (7.3) with (7.2). We see that

$$v_1^*\big|_{y_*=0} = -\frac{1}{\lambda}\frac{\mathrm{d}A_1^*}{\mathrm{d}x_*}, \quad v_2^*\big|_{y_*=0} = -\frac{1}{\lambda}\frac{\partial A_2^*}{\partial x_*}. \tag{7.4a,b}$$

Conditions (7.4*a*,*b*) are easily converted into conditions for the pressure. This is done by setting $y_* = 0$ in the second equation in (6.7) and in (6.10*b*). We have

$$\left.\frac{\partial p_1^*}{\partial y_*}\right|_{y_*=0} = \frac{1}{\lambda}\frac{\mathrm{d}^2 A_1^*}{\mathrm{d}x_*^2}, \quad \left.\frac{\partial p_2^*}{\partial y_*}\right|_{y_*=0} = \frac{1}{\lambda}\frac{\partial^2 A_2^*}{\partial x_*^2} + \frac{1}{\lambda}\rho_0'(\bar{t})\frac{\mathrm{d}^2 A_1^*}{\mathrm{d}x_*^2}. \tag{7.5a,b}$$

To complete the formulation of the boundary-value problem in the upper tier one needs to supplement (7.5*a*,*b*) with perturbation attenuation conditions

$$p_1^* \to 0, \quad p_2^* \to 0 \quad \text{as } x_*^2 + y_*^2 \to \infty. \tag{7.6}$$

7.1. *Steady flow*

To describe the steady perturbations produced in the flow by the wall roughness we need to analyse the flow in the lower tier simultaneously with the flow in the upper tier as these are in mutual interaction with one another. In the lower tier we have to solve (6.15) subject to the boundary conditions (6.16)–(6.19). In the upper tier the flow is governed by equation (6.8) which should be solved with the boundary conditions on p_1^* in (7.5*a*,*b*) and (7.6). Considered together these equations and boundary conditions constitute the steady viscous–inviscid interaction problem. This problem involves four parameters: the dimensionless skin friction immediately before the interaction region λ, the fluid density ρ_w and viscosity coefficient μ_w on the body surface and the 'compressibility' parameter $\beta = \sqrt{1 - M_\infty^2}$. We perform the substitution of variables

$$\left.\begin{aligned} x_* &= \frac{\mu_w^{-1/4}\rho_w^{-1/2}}{\lambda^{5/4}\beta^{3/4}}\,\bar{X}, \quad Y_* = \frac{\mu_w^{1/4}\rho_w^{-1/2}}{\lambda^{3/4}\beta^{1/4}}\,\bar{Y} + F(x_*), \\ U_1^* &= \frac{\mu_w^{1/4}\rho_w^{-1/2}}{\lambda^{-1/4}\beta^{1/4}}\,\bar{U}_1, \quad V_1^* = \frac{\mu_w^{3/4}\rho_w^{-1/2}}{\lambda^{-3/4}\beta^{-1/4}}\,\bar{V}_1 + U_1^*\frac{\mathrm{d}F}{\mathrm{d}x_*}, \\ P_1^* &= \frac{\mu_w^{1/2}}{\lambda^{-1/2}\beta^{1/2}}\,\bar{P}_1, \quad A_1^* = \frac{\mu_w^{1/4}\rho_w^{-1/2}}{\lambda^{-1/4}\beta^{1/4}}\,\bar{A}_1 - \lambda F(x_*), \end{aligned}\right\} \tag{7.7}$$

that combines standard affine transformations of the triple-deck theory with Prandtl's transposition. The latter introduces the body-fitted coordinates $(\bar{X}, \bar{Y})$ with $\bar{X}$ measured along the roughness contour and $\bar{Y}$ in the normal direction. Here, it is assumed that the roughness shape function can be expressed in the form

$$F = \frac{\mu_w^{1/4}\rho_w^{-1/2}}{\lambda^{3/4}\beta^{1/4}}\,\bar{F}, \tag{7.8}$$

where $\bar{F}(\bar{X})$ is independent of λ, ρ_w, μ_w and β.

As a result of transformations (7.7) equations (6.15) and boundary conditions (6.16)–(6.19) assume that form

$$\left.\begin{gathered} \bar{U}_1\frac{\partial \bar{U}_1}{\partial \bar{X}} + \bar{V}_1\frac{\partial \bar{U}_1}{\partial \bar{Y}} = -\frac{\mathrm{d}\bar{P}_1}{\mathrm{d}\bar{X}} + \frac{\partial^2 \bar{U}_1}{\partial \bar{Y}^2}, \\ \frac{\partial \bar{U}_1}{\partial \bar{X}} + \frac{\partial \bar{V}_1}{\partial \bar{Y}} = 0, \\ \bar{U}_1 = \bar{V}_1 = 0 \quad \text{at } \bar{Y} = 0, \\ \bar{U}_1 = \bar{Y} + \cdots \quad \text{as } \bar{X} \to -\infty, \\ \bar{U}_1 = \bar{Y} + \bar{A}_1(\bar{X}) + \cdots \quad \text{as } \bar{Y} \to \infty. \end{gathered}\right\} \tag{7.9}$$

Corresponding to (7.7) the upper tier variables are transformed as

$$y_* = \frac{\mu_w^{-1/4}\rho_w^{-1/2}}{\lambda^{5/4}\beta^{7/4}}\,\bar{y}, \quad p_1^* = \frac{\mu_w^{1/2}}{\lambda^{-1/2}\beta^{1/2}}\,\bar{p}_1. \tag{7.10a,b}$$

This turns equation (6.8) and boundary conditions for p_1^* in (7.5*a*,*b*) and (7.6) into

$$\left.\begin{aligned} \frac{\partial^2 \bar{p}_1}{\partial \bar{X}^2} + \frac{\partial^2 \bar{p}_1}{\partial \bar{y}^2} &= 0, \\ \left.\frac{\partial \bar{p}_1}{\partial \bar{y}}\right|_{\bar{y}=0} &= \frac{\mathrm{d}^2 \bar{A}_1}{\mathrm{d}\bar{X}^2} - \frac{\mathrm{d}^2 \bar{F}}{\mathrm{d}\bar{X}^2}, \\ \bar{p}_1 \to 0 \quad &\text{as } \bar{X}^2 + \bar{y}^2 \to \infty. \end{aligned}\right\} \tag{7.11}$$

7.2. *Unsteady perturbations*

To study the unsteady perturbations we need to consider (6.20) in the lower tier. These should be solved subject to boundary conditions (6.21)–(6.23). The transformations

$$\left.\begin{gathered} \bar{t} = \frac{\mu_w^{-1/2}}{\lambda^{3/2}\beta^{1/2}} T, \quad \omega = \frac{\mu_w^{1/2}}{\lambda^{-3/2}\beta^{-1/2}} \bar{\omega}, \\ U_2^* = \frac{\mu_w^{1/4}\rho_w^{-1/2}}{\lambda^{-1/4}\beta^{1/4}} \bar{U}_2, \quad V_2^* = \frac{\mu_w^{3/4}\rho_w^{-1/2}}{\lambda^{-3/4}\beta^{-1/4}} \bar{V}_2 + U_2^* \frac{\mathrm{d}F}{\mathrm{d}x_*}, \\ P_2^* = \frac{\mu_w^{1/2}}{\lambda^{-1/2}\beta^{1/2}} \bar{P}_2, \quad A_2^* = \frac{\mu_w^{1/4}\rho_w^{-1/2}}{\lambda^{-1/4}\beta^{1/4}} \bar{A}_2 \end{gathered}\right\} \tag{7.12}$$

turn (6.20)–(6.23) into

$$\left.\begin{gathered} \frac{\partial \bar{U}_2}{\partial T} + \bar{U}_1 \frac{\partial \bar{U}_2}{\partial \bar{X}} + \bar{U}_2 \frac{\partial \bar{U}_1}{\partial \bar{X}} + \bar{V}_1 \frac{\partial \bar{U}_2}{\partial \bar{Y}} + \bar{V}_2 \frac{\partial \bar{U}_1}{\partial \bar{Y}} = -\frac{\partial \bar{P}_2}{\partial \bar{X}} + \frac{\partial^2 \bar{U}_2}{\partial \bar{Y}^2}, \\ \frac{\partial \bar{U}_2}{\partial \bar{X}} + \frac{\partial \bar{V}_2}{\partial \bar{Y}} = 0, \\ \bar{U}_2 = \bar{V}_2 = 0 \quad \text{at } \bar{Y} = 0, \\ \bar{U}_2 = 0 \quad \text{at } \bar{X} = -\infty, \\ \bar{U}_2 = \bar{A}_2(T, \bar{X}) + \cdots \quad \text{as } \bar{Y} \to \infty. \end{gathered}\right\} \tag{7.13}$$

In the upper tier the unsteady perturbations are governed by (6.11). It should be solved subject to boundary conditions on p_2^* in (7.5*a*,*b*) and (7.6). The affine transformations

$$y_* = \frac{\mu_w^{-1/4}\rho_w^{-1/2}}{\lambda^{5/4}\beta^{7/4}} \bar{y}, \quad p_2^* = \frac{\mu_w^{1/2}}{\lambda^{-1/2}\beta^{1/2}} \bar{p}_2 \tag{7.14a,b}$$

turn the upper tier problem into

$$\left.\begin{aligned} \frac{\partial^2 \bar{p}_2}{\partial \bar{X}^2} + \frac{\partial^2 \bar{p}_2}{\partial \bar{y}^2} &= \rho_0'(T) \frac{M_\infty^2}{1 - M_\infty^2} \frac{\partial^2 \bar{p}_1}{\partial \bar{X}^2}, \\ \left.\frac{\partial \bar{p}_2}{\partial \bar{y}}\right|_{\bar{y}=0} &= \frac{\partial^2 \bar{A}_2}{\partial \bar{X}^2} + \rho_0'(T) \left(\frac{\mathrm{d}^2 \bar{A}_1}{\mathrm{d}\bar{X}^2} - \frac{\mathrm{d}^2 \bar{F}}{\mathrm{d}\bar{X}^2} \right), \\ \bar{p}_2 \to 0 \quad &\text{as } \bar{X}^2 + \bar{y}^2 \to \infty. \end{aligned}\right\} \tag{7.15}$$

Here, we write $\rho_0'(T)$ as

$$\rho_0'(T) = \rho_\alpha \mathrm{e}^{\mathrm{i}\bar{\omega}T}. \tag{7.16}$$

8. Linear receptivity

Modern requirements on the quality of the surface of a passenger aircraft make typical roughness rather shallow, which allows us to write

$$\bar{F} = hf(\bar{X}), \tag{8.1}$$

where h is a small parameter and $f(\bar{X})$ is an order-one function.

We start with the steady flow past the roughness. In the lower tier it is described by (7.9). In the case of shallow roughness (8.1) the solution to (7.9) is sought in the form

$$\left.\begin{aligned} \bar{U}_1 &= \bar{Y} + hU_1(\bar{X}, \bar{Y}) + \cdots, \quad \bar{V}_1 = hV_1(\bar{X}, \bar{Y}) + \cdots, \\ \bar{P}_1 &= hP_1(\bar{X}) + \cdots, \quad \bar{A}_1 = hA_1(\bar{X}) + \cdots. \end{aligned}\right\} \tag{8.2}$$

Functions U_1, V_1, P_1 and A_1 are found by making use of a standard routine first used by Stewartson (1970), see also § 5.1 in Ruban *et al.* (2013). The solution is expressed in the form

$$\breve{A}_1(k) = \frac{(\mathrm{i}k)^{1/3}|k|}{(\mathrm{i}k)^{1/3}|k| - 3Ai'(0)}\breve{f}(k). \tag{8.3}$$

Here, $\breve{A}_1(k)$ is the Fourier transform of the displacement function $A_1(\bar{X})$ defined as

$$\breve{A}_1(k) = \int_{-\infty}^{\infty} A_1(\bar{X})\mathrm{e}^{-\mathrm{i}k\bar{X}}\,\mathrm{d}\bar{X}, \tag{8.4}$$

where $Ai'(0)$ is the derivative of the Airy function at zero value of the argument, and $\breve{f}(k)$ is the Fourier transform of the roughness shape function $f(\bar{X})$. The solution for the pressure p_1 in the upper tier is expressed in terms of the Fourier transforms as

$$\breve{p}_1(k, \bar{y}) = \frac{3Ai'(0)}{(\mathrm{i}k)^{1/3}|k| - 3Ai'(0)}|k|\breve{f}(k)\,\mathrm{e}^{-|k|\bar{y}}. \tag{8.5}$$

Now we turn to the unsteady perturbations that are governed by (7.13) and (7.15). Keeping in mind that the forcing caused by the entropy waves is periodic in time, we represent the solution in the lower tier in the form

$$\left.\begin{aligned} \bar{U}_2 &= h\rho_\alpha \mathrm{e}^{\mathrm{i}\bar{\omega}T}U_2(\bar{X}, \bar{Y}) + (\text{c.c.}), \quad \bar{V}_2 = h\rho_\alpha \mathrm{e}^{\mathrm{i}\bar{\omega}T}V_2(\bar{X}, \bar{Y}) + (\text{c.c.}), \\ \bar{P}_2 &= h\rho_\alpha \mathrm{e}^{\mathrm{i}\bar{\omega}T}P_2(\bar{X}) + (\text{c.c.}), \quad \bar{A}_2 = h\rho_\alpha \mathrm{e}^{\mathrm{i}\bar{\omega}T}A_2(\bar{X}) + (\text{c.c.}). \end{aligned}\right\} \tag{8.6}$$

This turns (7.13) into

$$\left.\begin{aligned} \mathrm{i}\bar{\omega}U_2 + \bar{Y}\frac{\partial U_2}{\partial \bar{X}} + V_2 &= -\frac{\mathrm{d}P_2}{\mathrm{d}\bar{X}} + \frac{\partial^2 U_2}{\partial \bar{Y}^2}, \\ \frac{\partial U_2}{\partial \bar{X}} + \frac{\partial V_2}{\partial \bar{Y}} &= 0, \\ U_2 = V_2 &= 0 \quad \text{at } \bar{Y} = 0, \\ U_2 &\to 0 \quad \text{as } \bar{X} \to -\infty, \\ U_2 &= A_2(\bar{X}) \quad \text{at } \bar{Y} = \infty. \end{aligned}\right\} \tag{8.7}$$

Correspondingly, in the upper tier the solution is sought in the form

$$\bar{p}_2 = h\rho_\alpha \mathrm{e}^{\mathrm{i}\bar{\omega}T}p_2(\bar{X}, \bar{y}) + (\text{c.c.}), \tag{8.8}$$

which turns (7.15) into

$$\left.\begin{aligned} \frac{\partial^2 p_2}{\partial \bar{X}^2}+\frac{\partial^2 p_2}{\partial \bar{y}^2}&=\frac{M_\infty^2}{1-M_\infty^2}\frac{\partial^2 p_1}{\partial \bar{X}^2},\\ \left.\frac{\partial p_2}{\partial \bar{y}}\right|_{\bar{y}=0}&=\frac{\partial^2 A_2}{\partial \bar{X}^2}+\frac{\mathrm{d}^2 A_1}{\mathrm{d}\bar{X}^2}-\frac{\mathrm{d}^2 f}{\mathrm{d}\bar{X}^2},\\ p_2&\to 0 \quad \text{as } \bar{X}^2+\bar{y}^2\to\infty. \end{aligned}\right\} \tag{8.9}$$

The solutions in the upper and lower tiers are linked to one another through the requirement that

$$P_2 = p_2|_{\bar{y}=0}\,. \tag{8.10}$$

The boundary-value problem for the upper tier (8.9) is expressed in terms of Fourier transforms as

$$\frac{\mathrm{d}^2\breve{p}_2}{\mathrm{d}\bar{y}^2}-k^2\breve{p}_2=\Lambda\breve{f}(k)\,\mathrm{e}^{-|k|\bar{y}}, \tag{8.11a}$$

$$\left.\frac{\mathrm{d}\breve{p}_2}{\mathrm{d}\bar{y}}\right|_{\bar{y}=0}=-k^2(\breve{A}_2+\breve{A}_1-\breve{f}), \tag{8.11b}$$

$$\breve{p}_2\to 0 \quad \text{as } \bar{y}\to\infty. \tag{8.11c}$$

The forcing term on the right-hand side of (8.11*a*) is obtained using the solution (8.5) for $\breve{p}_1$. It is found that the constant Λ is given by

$$\Lambda=-\frac{M_\infty^2}{1-M_\infty^2}\frac{3k^2|k|Ai'(0)}{(\mathrm{i}k)^{1/3}|k|-3Ai'(0)}. \tag{8.12}$$

The solution to the boundary-value problem (8.11) is written as

$$\breve{p}_2=\left[|k|(\breve{A}_2+\breve{A}_1-\breve{f})-\frac{\Lambda}{2k^2}\breve{f}(k)\right]\mathrm{e}^{-|k|\bar{y}}-\frac{\Lambda}{2|k|}\breve{f}(k)\bar{y}\mathrm{e}^{-|k|\bar{y}}. \tag{8.13}$$

It remains to set $\bar{y}=0$ and we will find that the Fourier transform of the pressure P_2 in the lower tier is given by

$$\breve{P}_2=|k|(\breve{A}_2+\breve{A}_1)-\left(|k|+\frac{\Lambda}{2k^2}\right)\breve{f}(k). \tag{8.14}$$

The equations for the lower tier (8.7) are written in terms of the Fourier transforms as

$$\mathrm{i}\bar{\omega}\breve{U}_2+\mathrm{i}k\bar{Y}\breve{U}_2+\breve{V}_2=-\mathrm{i}k\breve{P}_2+\frac{\mathrm{d}^2\breve{U}_2}{\mathrm{d}\bar{Y}^2}, \tag{8.15a}$$

$$\mathrm{i}k\breve{U}_2+\frac{\mathrm{d}\breve{V}_2}{\mathrm{d}\bar{Y}}=0, \tag{8.15b}$$

$$\breve{U}_2=\breve{V}_2=0 \quad \text{at } \bar{Y}=0, \tag{8.15c}$$

$$\breve{U}_2=\breve{A}_2(\bar{X}) \quad \text{at } \bar{Y}=\infty. \tag{8.15d}$$

We start the solution of the boundary-value problem (8.15) by eliminating $\breve{V}_2$ from (8.15*a*) and (8.15*b*). For this purpose, we differentiate the momentum equation (8.15*a*)

with respect to $\bar{Y}$ and then, using the continuity equation (8.15*b*), we find that $\breve{U}_2$ satisfies the equation

$$\mathrm{i}(\bar{\omega} + k\bar{Y})\frac{\mathrm{d}\breve{U}_2}{\mathrm{d}\bar{Y}} = \frac{\mathrm{d}^3\breve{U}_2}{\mathrm{d}\bar{Y}^3}. \tag{8.16}$$

Since this is a third-order differential equation, it requires an additional boundary condition. The latter may be obtained by setting $\bar{Y} = 0$ in (8.15*a*). We have

$$\left.\frac{\mathrm{d}^2\breve{U}_2}{\mathrm{d}\bar{Y}^2}\right|_{\bar{Y}=0} = \mathrm{i}k\breve{P}_2. \tag{8.17}$$

If we now introduce a new independent variable

$$z = z_0 + \theta\bar{Y}, \tag{8.18}$$

with

$$z_0 = \frac{\bar{\omega}}{k}\theta, \quad \theta = (\mathrm{i}k)^{1/3}, \tag{8.19}$$

then (8.16) turns into the Airy equation for the derivative $\mathrm{d}\breve{U}_2/\mathrm{d}z$

$$\frac{\mathrm{d}^3\breve{U}_2}{\mathrm{d}z^3} - z\frac{\mathrm{d}\breve{U}_2}{\mathrm{d}z} = 0. \tag{8.20a}$$

The boundary conditions (8.15*c*), (8.15*d*) and (8.17) are written in the new variables as

$$\breve{U}_2 = 0 \quad \text{at } z = z_0, \tag{8.20b}$$

$$\frac{\mathrm{d}^2\breve{U}_2}{\mathrm{d}z^2} = (\mathrm{i}k)^{1/3}\breve{P}_2 \quad \text{at } z = z_0, \tag{8.20c}$$

$$\breve{U}_2 = \breve{A}_2 \quad \text{at } z = \infty. \tag{8.20d}$$

The general solution of (8.20*a*) is

$$\frac{\mathrm{d}\breve{U}_2}{\mathrm{d}z} = C_1 Ai(z) + C_2 Bi(z), \tag{8.21}$$

where $Ai(z)$ is the Airy function that decays exponentially as $z \to \infty$, while $Bi(z)$ is exponentially growing for all k in the complex plane, provided that the branch cut in this plane is made along the positive imaginary semi-axis (see figure 8). It follows from (8.20*d*) that $\breve{U}_2$ should remain bounded. Therefore, we have to set $C_2 = 0$, and we can conclude that

$$\frac{\mathrm{d}\breve{U}_2}{\mathrm{d}z} = C_1 Ai(z). \tag{8.22}$$

Substitution of (8.22) into (8.20*c*) results in

$$C_1 Ai'(z_0) = (\mathrm{i}k)^{1/3}\breve{P}_2. \tag{8.23}$$

Let us now integrate (8.22) with initial condition (8.20*b*). We have

$$\breve{U}_2 = C_1 \int_{z_0}^{z} Ai(\zeta)\,\mathrm{d}\zeta. \tag{8.24}$$

Setting $z = \infty$ in the above equation, and using condition (8.20*d*) we find that

$$C_1 \int_{z_0}^{\infty} Ai(z)\,\mathrm{d}z = \breve{A}_2. \tag{8.25}$$

It remains to eliminate C_1 from (8.25) and (8.23), and we will have

$$\breve{A}_2 = \frac{(\mathrm{i}k)^{1/3}\breve{P}_2}{Ai'(z_0)} \int_{z_0}^{\infty} Ai(z)\,\mathrm{d}z. \tag{8.26}$$

This is the second equation relating $\breve{A}_2$ and $\breve{P}_2$. The first one is given by the solution (8.14) for the upper tier. Elimination of $\breve{A}_2$ from (8.14) and (8.26) results in

$$\breve{P}_2 = \frac{Ai'(z_0)}{Q(\bar{\omega}, k)} \left\{ |k|[\breve{A}_1 - \breve{f}(k)] - \frac{\Lambda}{2k^2}\breve{f}(k) \right\}, \tag{8.27}$$

where

$$Q(\bar{\omega}, k) = Ai'(z_0) - (\mathrm{i}k)^{1/3}|k| \int_{z_0}^{\infty} Ai(z)\,\mathrm{d}z. \tag{8.28}$$

It remains to substitute (8.3) and (8.12) into (8.27) and we arrive at a conclusion that the Fourier transform of the pressure in the lower tier is

$$\breve{P}_2 = \frac{Ai'(z_0)}{Q(\bar{\omega}, k)} \left[\frac{3(1+D)Ai'(0)|k|}{(\mathrm{i}k)^{1/3}|k| - 3Ai'(0)} \right] \breve{f}(k), \tag{8.29}$$

where

$$D = \frac{M_\infty^2}{2(1 - M_\infty^2)}. \tag{8.30}$$

To return to physical variables we need to apply the inverse Fourier transform to (8.29). Substituting the result into the equation for $\bar{P}_2$ in (8.6) we have

$$\bar{P}_2(T, \bar{X}) = h\rho_\alpha \frac{\mathrm{e}^{\mathrm{i}\bar{\omega}T}}{2\pi} \int_{-\infty}^{\infty} \frac{Ai'(z_0)}{Q(\bar{\omega}, k)} \left[\frac{3(1+D)Ai'(0)|k|}{(\mathrm{i}k)^{1/3}|k| - 3Ai'(0)} \right] \breve{f}(k) \mathrm{e}^{\mathrm{i}k\bar{X}}\,\mathrm{d}k + (\text{c.c.}). \tag{8.31}$$

In the receptivity theory, our main interest is in the behaviour of the solution behind the wall roughness. The analysis presented in Appendix A shows that

$$\begin{aligned} \bar{P}_2(T, \bar{X}) &= h\rho_\alpha \mathcal{K}(\bar{\omega}) \breve{f}(k_1) \exp\left(\mathrm{i}(k_1\bar{X} + \bar{\omega}T)\right) \\ &+ h\rho_\alpha \frac{1+D}{\pi} \breve{f}(0) \frac{\mathrm{e}^{\mathrm{i}\bar{\omega}T}}{\bar{X}^2} + \cdots + (\text{c.c.}) \quad \text{as } \bar{X} \to \infty. \end{aligned} \tag{8.32}$$

The Tollmien–Schlichting wave generated through the interaction of the entropy wave with a wall roughness is represented by the first term on the right-hand side of (8.32). The amplitude of the Tollmien–Schlichting wave is proportional to the receptivity coefficient $\mathcal{K}(\bar{\omega})$ and the Fourier transform $\breve{f}(k_1)$ of the roughness shape function $f(\bar{X})$ calculated for the wavenumber k_1 which is the wavenumber of the Tollmien–Schlichting wave for a given

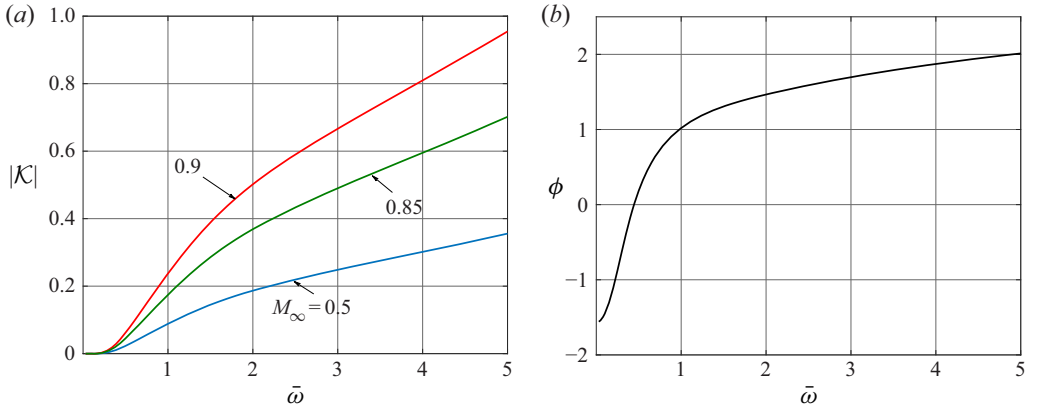

Figure 4. The receptivity coefficient $\mathcal{K} = |\mathcal{K}|e^{i\phi}$ as a function of the frequency $\bar{\omega}$ for various values of the Mach number M_∞. (*a*) Modulus of the receptivity coefficient. (*b*) Argument of the receptivity coefficient.

frequency $\bar{\omega}$ of the entropy wave. The receptivity coefficient is calculated as

$$\mathcal{K}(\bar{\omega}) = \left[\frac{Ai'(z_0)}{\partial Q/\partial k}\,\frac{3i(1+D)Ai'(0)k}{(ik)^{1/3}k + 3Ai'(0)}\right]_{k=k_1}, \tag{8.33}$$

with $\partial Q/\partial k$ given by (A10) and D by (8.30). Notice that $\mathcal{K}$ is a function of the frequency $\bar{\omega}$ and the Mach number M_∞ only.

The numerical calculations of $\mathcal{K}(\bar{\omega})$ were performed in the following way. Firstly, a real value of the frequency $\bar{\omega}$ is chosen. The corresponding values of k and z_0 are given by the first root k_1 of the dispersion equation (A5) which was solved with the help of Newtonian iterations. When performing the iterations, the values of the Airy function, its derivative and the integral at the point z_0 in the complex z-plane were found by solving the initial-value problem for the Airy equation along a straight line connecting the origin $z = 0$ and $z = z_0$ with the Airy function $Ai(0)$ and its derivative $Ai'(0)$ assigned the well-known values at $z = 0$. The results of the calculations are displayed in figure 4. Notice that the argument ϕ of the receptivity coefficient is independent of the Mach number.

9. Nonlinear receptivity

The linear receptivity analysis presented in the previous section relies on the assumption that the wall roughness is shallow, that is, the roughness shape function $\bar{F}(\bar{X})$ may be expressed in the form (8.1) with the height parameter h assumed small. Under this assumption, the steady flow past the roughness is only slightly perturbed which preclude the situations when the flow involves a separation.

We shall now lift this restriction and extend the theory to the case when $\bar{F}(\bar{X})$ is an order-one quantity. In this case both the steady flow problem (7.9), (7.11) and the problem (7.13), (7.15) for unsteady perturbations require numerical solution. We used for this purpose numerical technique developed by Kravtsova, Zametaev & Ruban (2005). Some of the computation results are shown in figure 5. We chose the shape of the roughness to be $\bar{F} = he^{-2\bar{X}^2}$. Figure 5 displays the streamlines in the viscous sublayer for different values of the height parameter h. We found that the separation region formed when h was close to $h = 2.5$. The separation region increases in size as h is growing.

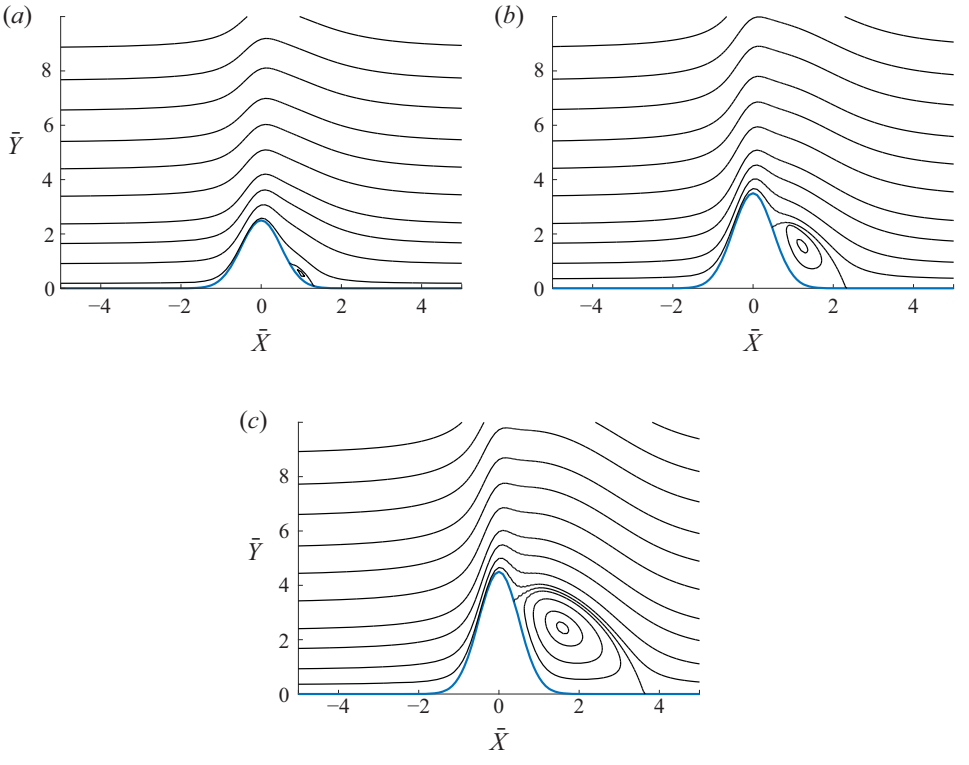

Figure 5. Streamlines for the steady separated flow around a roughness; (*a*) $h = 2.5$, (*b*) $h = 3.5$, (*c*) $h = 4.5$.

When dealing with unsteady perturbations, we modified the numerical technique of Kravtsova *et al.* (2005) as follows. We note that the forcing terms in (7.15), both in the equation for $\bar{p}_2$ and in the boundary condition at $\bar{y} = 0$, are periodic functions of time with frequency $\bar{\omega}$. We therefore represent the solution to (7.13) in the form

$$\left.\begin{aligned} \bar{U}_2 &= \rho_\alpha \left[U_{21}\sin(\bar{\omega}T) + U_{22}\cos(\bar{\omega}T)\right], \\ \bar{V}_2 &= \rho_\alpha \left[V_{21}\sin(\bar{\omega}T) + V_{22}\cos(\bar{\omega}T)\right], \\ \bar{P}_2 &= \rho_\alpha \left[P_{21}\sin(\bar{\omega}T) + P_{22}\cos(\bar{\omega}T)\right], \\ \bar{A}_2 &= \rho_\alpha \left[A_{21}\sin(\bar{\omega}T) + A_{22}\cos(\bar{\omega}T)\right]. \end{aligned}\right\} \tag{9.1}$$

The substitution of (9.1) into (7.13) results in the following set of linear equations:

$$\left.\begin{aligned} -\bar{\omega}U_{22} + \bar{U}_1\frac{\partial U_{21}}{\partial \bar{X}} + U_{21}\frac{\partial \bar{U}_1}{\partial \bar{X}} + \bar{V}_1\frac{\partial U_{21}}{\partial \bar{Y}} + V_{21}\frac{\partial \bar{U}_1}{\partial \bar{Y}} &= -\frac{\partial P_{21}}{\partial \bar{X}} + \frac{\partial^2 U_{21}}{\partial \bar{Y}^2}, \\ \bar{\omega}U_{21} + \bar{U}_1\frac{\partial U_{22}}{\partial \bar{X}} + U_{22}\frac{\partial \bar{U}_1}{\partial \bar{X}} + \bar{V}_1\frac{\partial U_{22}}{\partial \bar{Y}} + V_{22}\frac{\partial \bar{U}_1}{\partial \bar{Y}} &= -\frac{\partial P_{22}}{\partial \bar{X}} + \frac{\partial^2 U_{22}}{\partial \bar{Y}^2}, \\ \frac{\partial U_{21}}{\partial \bar{X}} + \frac{\partial V_{21}}{\partial \bar{Y}} = 0, \quad \frac{\partial U_{22}}{\partial \bar{X}} + \frac{\partial V_{22}}{\partial \bar{Y}} &= 0. \end{aligned}\right\} \tag{9.2}$$

These have to be solved subject to the boundary conditions

$$\left.\begin{aligned} &U_{21} = U_{22} = V_{21} = V_{22} = 0 \quad \text{at } \bar{Y} = 0, \\ &U_{21} = A_{21}(\bar{X}), \quad U_{22} = A_{22}(\bar{X}) \quad \text{at } \bar{Y} = \infty, \\ &U_{21} = U_{22} = 0 \quad \text{at } \bar{X} = -\infty. \end{aligned}\right\} \tag{9.3}$$

To perform the calculations, we introduce a discrete mesh $\{\bar{X}_i\}$, where $i = 1, 2, \ldots, N$, and denote the vector composed of the values of the displacement function $A(\bar{X})$ at the mesh points by $\boldsymbol{A}$, namely,

$$\boldsymbol{A} = \left\{A_{21}(\bar{X}_1),\, A_{21}(\bar{X}_2), \ldots, A_{21}(\bar{X}_N),\, A_{22}(\bar{X}_1),\, A_{22}(\bar{X}_2), \ldots, A_{22}(\bar{X}_N)\right\}. \tag{9.4}$$

We also consider the pressure gradient vector $\mathrm{d}\boldsymbol{P}/\mathrm{d}x$ whose elements are calculated in the same way. For given displacement function $\boldsymbol{A}$, equations (9.2), (9.3) allow us to calculate the velocity field and the pressure gradient in the viscous sublayer, leading to the matrix equation

$$\left.\frac{\mathrm{d}\boldsymbol{P}}{\mathrm{d}x}\right|_{visc} = \boldsymbol{M}\boldsymbol{A}, \tag{9.5}$$

where $\boldsymbol{M}$ is $2N \times 2N$ matrix.

The finite-difference representation of inviscid equations (7.15) can be expressed in the form

$$\left.\frac{\mathrm{d}\boldsymbol{P}}{\mathrm{d}x}\right|_{inv} = \boldsymbol{N}\boldsymbol{A} + \boldsymbol{R}, \tag{9.6}$$

with the vector $\boldsymbol{R}$ representing the forcing terms in (7.15).

The requirement that the pressure gradient should be the same in the viscous sublayer and at the bottom of the upper deck leads to the following set of linear equations:

$$(\boldsymbol{M} - \boldsymbol{N})\boldsymbol{A} = \boldsymbol{R}. \tag{9.7}$$

An interested reader is referred to the original paper by Kravtsova *et al.* (2005) for the details of numerical calculation of matrices $\boldsymbol{M}$ and $\boldsymbol{N}$.

The results of unsteady flow calculations at different values of the free-stream Mach number M_∞ are shown in figure 6 in the form of the pressure gradient oscillations along the body surface. Upstream of the wall roughness the perturbations decay very fast, but they persist behind the roughness assuming the form of a Tollmien–Schlichting wave. According to the linear theory, the neutral frequency of the Tollmien–Schlichting wave is $\bar{\omega} = 2.3$. Since for all values of h, the steady flow downstream of the roughness returns to its unperturbed state $\bar{U}_1 = \bar{Y}$, the neutral frequency $\bar{\omega}$ should not change with h, and figure 6 does confirm this expectation. Indeed, we see that for this frequency, the oscillations neither grow nor decay downstream of the roughness.

As far as the amplitude of the oscillations is concerned, it increases rather rapidly with h, as figures 6(*a*)–6(*c*) clearly show. In figure 7 we show the effect of nonlinearity on the receptivity coefficient $|\mathcal{K}|$. The latter is calculated as the ratio of the amplitude of the generated Tollmien–Schlichting wave and the roughness height h. We see that $|\mathcal{K}|$ increases with h first slowly but then, when the separation develops in the flow (see figure 5), much faster. We also see that the receptivity coefficient increases with the Mach number, which tells us that the generation of the Tollmien–Schlichting waves by the entropy waves should not be ignored when predicting the laminar–turbulent transition on a passenger aircraft wing in cruise flight.

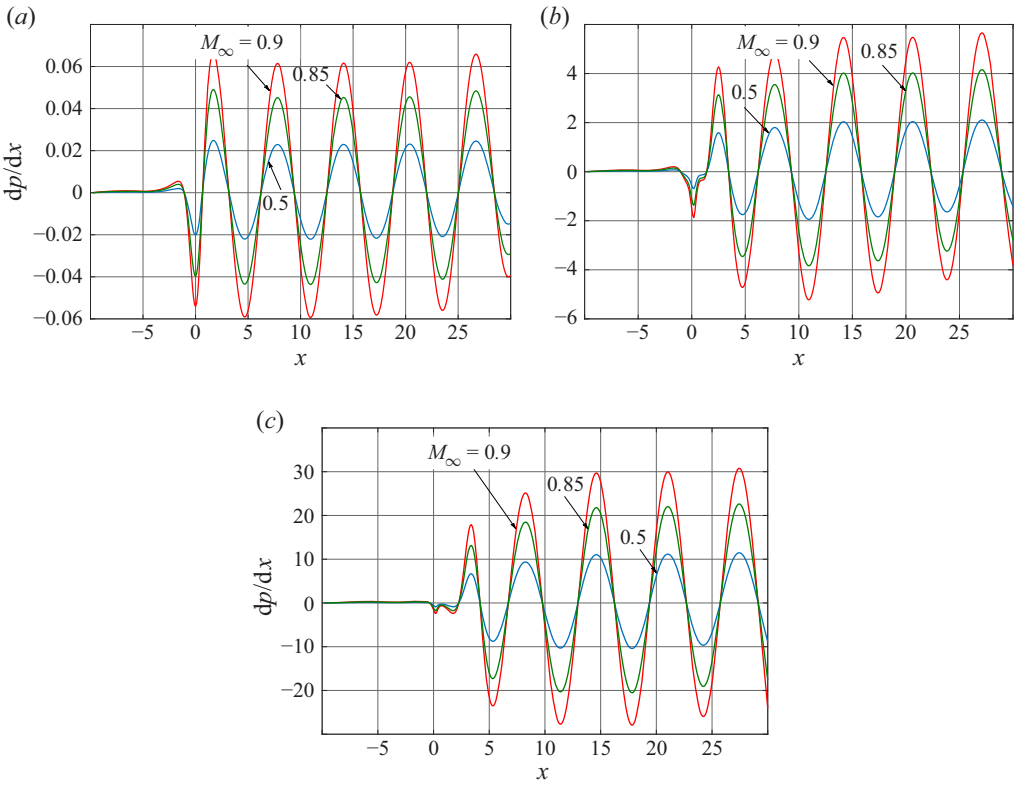

Figure 6. Perturbations of pressure gradient for (*a*) $h = 0.1$; (*b*) $h = 3.5$; (*c*) $h = 4.5$. In all three cases, the neutral frequency, $\bar{\omega} = 2.3$, is taken.

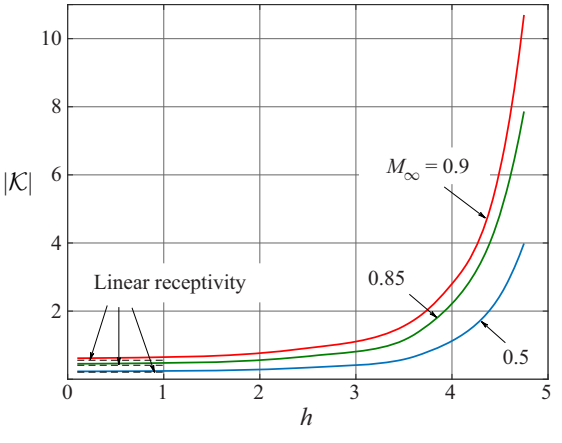

Figure 7. Receptivity coefficient, $|\mathcal{K}|$, as a function of the roughness height, h, for various values of the Mach number, M_∞; dashed lines correspond to the linear receptivity predictions.

10. Concluding remarks

In this paper we consider the generation of the Tollmien–Schlichting waves in the boundary layer due to the presence of the entropy waves in the oncoming free-stream flow. It is well known that in compressible flows, small perturbations to a uniform

free-stream flow can be decomposed into acoustic waves and the free-stream turbulence. The latter consists of two perturbation modes: the vorticity waves and the entropy waves. The receptivity of the boundary layer to acoustic noise and to the vorticity waves has been studied extensively by various authors. The entropy waves did not attract such attention, except for hypersonic flows. In the present paper our attention is with the receptivity of the boundary layer to entropy waves in subsonic flows. Since in aerodynamic applications, the Tollmien–Schlichting waves are observed at relatively large values of the Reynolds number, Re, the asymptotic solution of the Navier–Stokes equations was used for a theoretical description of the receptivity process. We assumed that in the spectrum of the entropy waves there are harmonics which come in resonance with the Tollmien–Schlichting wave on the lower branch of the stability curve; this happens when the frequency, ω, is an order $Re^{1/4}$ quantity, but since the speed of propagation of the entropy wave coincides with the free-stream velocity, the wavelength appears to be $O(Re^{1/4})$ long, which is much longer than the wavelength of the Tollmien–Schlichting wave. Hence, to satisfy the resonance condition with respect to the wavenumber, the entropy wave has to come into interaction with the wall roughness, which are, of course, plentiful on a real aircraft wing.

We first analysed the interaction of the entropy wave with the boundary layer before the roughness. The entropy waves produce oscillations of the gas temperature and density, but the velocity and pressure remain unperturbed to the leading order. This precludes the entropy waves from penetrating the boundary layer. Instead, they decay very rapidly in the transition layer situated near the outer edge of the conventional boundary layer. As a result of this, there is a significant difference in the way the boundary layer interacts with entropy waves compared with the acoustic waves. The acoustic waves carry pressure perturbations which easily penetrate into the boundary layer and lead to a formation of the Stokes layer near the body surface; this is due to the Stokes layer interaction with steady perturbations near the wall roughness that the Tollmien–Schlichting waves form in the boundary layer. The situation with the entropy waves is different. They do not create the Stokes layer on the wing surface. However, a wall roughness produces perturbations not only inside the boundary layer but also in the inviscid flow outside the boundary layer. The interaction of these perturbations with the entropy waves creates the forcing necessary for the Tollmien–Schlichting wave production.

To perform the analysis of the receptivity process, the triple-deck theory has been modified appropriately. The equations of the triple-deck theory were then solved analytically for the case of linear receptivity when the roughness height is relatively small. We also performed nonlinear receptivity analysis in the case when the roughness height is not small. For this case, the full numerical solution of the triple-deck equations is required. We found that the nonlinearity enhances the receptivity process significantly. The receptivity coefficient $\mathcal{K}$ was found to increase with the roughness height h first slowly but then, when the separation develops in the flow, $\mathcal{K}$ grows much faster. We also see that $\mathcal{K}$ increases with the Mach number. This means that the generation of the Tollmien–Schlichting waves by the entropy waves should be taken into account when predicting the laminar turbulent transition on a passenger aircraft wing in cruise flight.

As was demonstrated by Wu (2001), the predictions of the receptivity theory are in good agreement with the experimental observations. There is now also clear evidence that the asymptotic triple-deck theory is as accurate as numerical simulations based on the Navier–Stokes equations (see, for example, De Tullio & Ruban 2015). Compared with numerical methods, the theoretical predictions have obvious advantages. Firstly, the triple-deck theory allows us to deduce an explicit formula (8.32) for the amplitude of the

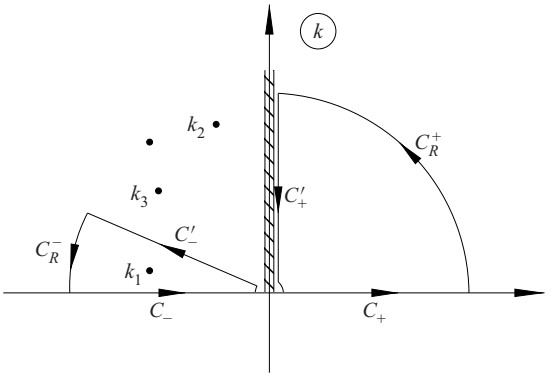

Figure 8. Integration contours.

generated Tollmien–Schlichting wave, which may be used, for example, if the receptivity process is to be suppressed in the flow near various technological dents or humps on an aircraft wing through passive or active flow control as in Brennan, Gajjar & Hewitt (2021). Secondly, the asymptotic theory represents an ideal tool for uncovering the physical processes leading to the generation of the instability modes in the boundary layer. Thirdly, the asymptotic theory proved to be instrumental in identifying possible mechanisms of the boundary-layer receptivity. These include the generation of Görtler vortices by wall roughness (see Denier, Hall & Seddougui 1991) as well as by the free-stream longitudinal vortices (see Wu, Zhao & Luo 2011). In the latter case, the instability modes form in the boundary layer without the aid of a wall roughness. Another example of this type of receptivity is presented in the paper by Wu (1999) devoted to the generation of the Tollmien–Schlichting waves due to the interaction of the free-stream turbulence with acoustic waves. In this paper, the concept of distributed receptivity was put forward, which was further developed in Wu (2001); see also Kerimbekov & Ruban (2005). The asymptotic receptivity theory can be adjusted to different flow speed regimes. In particular, Ruban, Bernots & Kravtsova (2016) studied with its help the receptivity of the boundary layer to acoustic waves in transonic flows and Dong, Liu & Wu (2020) performed the corresponding analysis for supersonic flows. The present paper is the first study where the triple-deck theory is applied to the receptivity of the boundary layer with respect to entropy waves.

Declaration of interests. The authors report no conflict of interest.

Author ORCIDs.
A.I. Ruban https://orcid.org/0000-0001-8853-8160.

Appendix A. Amplitude of the Tollmien–Schlichting wave

The integration in (8.31) is meant to be performed along the real axis in the complex k-plane. However, since our interest is in the behaviour of the solution downstream of the roughness, we shall consider an analytical extension of the integrand into the upper half of the complex k-plane, and change the contour of integration as shown in figure 8. When performing this task one needs to identify the poles in the region swept by the deforming contour.

We start with the real negative semi-axis, shown as C_- in figure 8. To make the integrand in (8.31) an analytic function we have to substitute $|k|$ by $-k$. It is easily shown that the

denominator of the expression in the square brackets in (8.31) cannot become zero in the second quadrant in the complex k-plane. Indeed, let us examine the equation

$$(ik)^{1/3}|k| + a = 0, \tag{A1}$$

where $a = -3Ai'(0) > 0$. Setting $|k| = -k$ and expressing k in the form $k = |k|e^{i\vartheta}$, where ϑ belongs to the interval

$$\vartheta \in \left(-\frac{3}{2}\pi, \frac{1}{2}\pi\right), \tag{A2}$$

we can write (A1) as

$$(e^{i\pi/2}|k|e^{i\vartheta})^{4/3} = ia. \tag{A3}$$

It follows from (A3) that

$$\vartheta = -\frac{1}{8}\pi + \frac{3}{2}\pi n, \quad n = 0, \pm1, \pm2, \ldots. \tag{A4}$$

We see that the only solution satisfying restriction (A2) is given by $n = 0$ for which $\vartheta = -\pi/8$. Clearly it does not belong to the second quadrant in the k-plane.

Similarly, (A1) can be analysed for the positive real semi-axis in the k-plane, where $|k| = k$. Again, no solution that belongs to the first quadrant is found.

Thus, the only singularities that have to be taken into account are those located points where $Q(\bar{\omega}, k)$ is zero. This leads to the following dispersion equation:

$$Ai'(z_0) - (ik)^{1/3}|k| \int_{z_0}^{\infty} Ai(z)\,dz = 0, \quad z_0 = \frac{\bar{\omega}}{k}(ik)^{1/3}. \tag{A5}$$

This equation was studied by various authors (see, for example, Zhuk & Ryzhov 1980), and it is known that it has an infinite (countable) number of roots. The position of each root in the complex k-plane depends on the frequency $\bar{\omega}$. The trajectories of the first five roots, as $\bar{\omega}$ changes from zero to infinity, are shown in figure 9. All the roots originate at $\bar{\omega} = 0$ from the coordinate origin ($k = 0$), and all of them, except the first one, remain in the second quadrant for all $\bar{\omega} \in (0, \infty)$, indicating that the corresponding perturbations in the boundary layer decay with x. The behaviour of the first root is different. It stays in the second quadrant until the frequency reaches its critical value, $\omega_* = 2.29797$, and then it crosses the real axis at the point $k_* = -1.00049$ and remains in the third quadrant for all $\bar{\omega} \in (\omega_*, \infty)$. This root represents the Tollmien–Schlichting wave; our task is to determine its amplitude.

Let us consider the frequency $\bar{\omega}$ which is smaller than the critical frequency, ω_*. Then all the roots of (A5) are represented by points that lie in the second quadrant of the complex k-plane, as shown in figure 9. Remember that when introducing an analytical branch of the function $(ik)^{1/3}$ we had to make a branch cut along the positive imaginary axis in the k-plane. Also, the analytical extension of $|k|$ in the integrand in (8.31) requires the branch cut to be extended to the entire imaginary axis. Therefore, we shall split the integration interval in (8.31) into two parts, the negative real semi-axis and the positive real semi-axis,

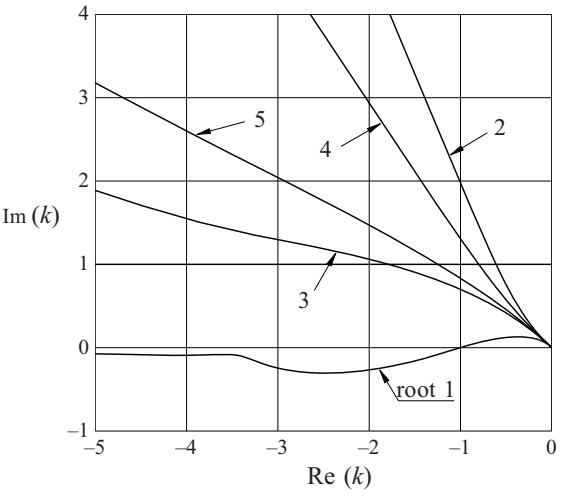

Figure 9. The first five roots of (A5) in the complex k-plane.

shown in figure 8 as C_- and C_+, respectively,

$$\bar{P}_2(T,\bar{X}) = h\rho_\alpha \frac{\mathrm{e}^{\mathrm{i}\bar{\omega}T}}{2\pi}\left\{\int_{-\infty}^{0}\mathcal{M}(k;\bar{\omega},\bar{X})\,\mathrm{d}k + \int_{0}^{\infty}\mathcal{N}(k;\bar{\omega},\bar{X})\,\mathrm{d}k\right\} + (\text{c.c.}). \tag{A6}$$

Here

$$\mathcal{M} = \frac{Ai'(z_0)}{Ai'(z_0) - \mathrm{i}(\mathrm{i}k)^{4/3}\int_{z_0}^{\infty}Ai(z)\,\mathrm{d}z}\left[\frac{3(1+D)Ai'(0)k}{(\mathrm{i}k)^{1/3}k + 3Ai'(0)}\right]\breve{f}(k)\mathrm{e}^{\mathrm{i}k\bar{X}}, \tag{A7}$$

and

$$\mathcal{N} = \frac{Ai'(z_0)}{Ai'(z_0) + \mathrm{i}(\mathrm{i}k)^{4/3}\int_{z_0}^{\infty}Ai(z)\,\mathrm{d}z}\left[\frac{3(1+D)Ai'(0)k}{(ik)^{1/3}k - 3Ai'(0)}\right]\breve{f}(k)\mathrm{e}^{\mathrm{i}k\bar{X}}. \tag{A8}$$

When calculating the first integral in (A6) we close the contour of integration by adding to C_- a ray C'_- and a circular arc C_R^- of a large radius R; see figure 8. If we choose the ray C'_- such that only the first root k_1 finds itself inside the combined contour then, using the Residue theorem, we will find that

$$\int_{C_-}\mathcal{M}\,\mathrm{d}k = 2\pi i\left[\frac{Ai'(z_0)}{\partial Q/\partial k}\,\frac{3(1+D)Ai'(0)k}{(\mathrm{i}k)^{1/3}k + 3Ai'(0)}\right]_{k=k_1}\breve{f}(k_1)\mathrm{e}^{\mathrm{i}k_1\bar{X}}$$
$$-\int_{C'_-}\mathcal{M}\,dk - \int_{C_R^-}\mathcal{M}\,\mathrm{d}k, \tag{A9}$$

where the derivative $\partial Q/\partial k$ of (8.28) is given by

$$\frac{\partial Q}{\partial k} = \frac{4}{3}(\mathrm{i}k)^{1/3}\int_{z_0}^{\infty}Ai(z)\,\mathrm{d}z - \frac{2}{3}\frac{z_0}{k}[z_0 + \mathrm{i}(ik)^{4/3}]Ai(z_0). \tag{A10}$$

Since $z_0 \to 0$ as $k \to \infty$, it is easily seen from (A7) that

$$\mathcal{M} \sim \frac{\breve{f}(k)}{k^{5/3}}\mathrm{e}^{\mathrm{i}k\bar{X}} \quad \text{as } k \to \infty, \tag{A11}$$

which means that Jordan's lemma is applicable to the integral along the arc C_R^- in (A9). According to this lemma, this integral tends to zero as the arc's radius R tends to infinity.

The behaviour of the integral along the ray C'_- may be evaluated using Watson's lemma. We find that

$$\int_{C'_-} \mathcal{M}\, dk = -(1+D)\breve{f}(0)\frac{1}{\bar{X}^2} + \cdots \quad \text{as } \bar{X} \to \infty. \tag{A12}$$

The second integral in (A6) is calculated in a similar way. We close the integration contour C_+ with a circular arc C_R^+ and a ray C'_+ that lies along the right-hand side of the branch cut; see figure 8. The integral along C_R^+ may be disregarded in view of Jordan's lemma. Taking further into account that there are no roots of the dispersion equation (A5) in the first quadrant of the k-plane, we can write

$$\int_{C_+} \mathcal{N}\, \mathrm{d}k = -\int_{C'_+} \mathcal{N}\, \mathrm{d}k. \tag{A13}$$

The integral on the right-hand side of (A13) is a Laplace type integral. It may be evaluated using Watson's lemma. We find that

$$\int_{C'_+} \mathcal{N}\, dk = -(1+D)\breve{f}(0)\frac{1}{\bar{X}^2} + \cdots \quad \text{as } \bar{X} \to \infty. \tag{A14}$$

It remains to substitute (A12) and (A14) into (A9) and (A13), respectively, and then into (A6). We find that downstream of the roughness, the pressure $\bar{P}_2(T, \bar{X})$ is given by (8.32).

References

Brennan, G.S., Gajjar, J.S.B. & Hewitt, R.E. 2021 Tollmien–Schlichting wave cancellation via localised heating elements in boundary layers. *J. Fluid Mech.* **909**, A16.

De Tullio, N. & Ruban, A.I. 2015 A numerical evaluation of the asymptotic theory of receptivity for subsonic compressible boundary layers. *J. Fluid Mech.* **771**, 520–546.

Denier, J.P., Hall, P. & Seddougui, S.O. 1991 On the receptivity problem for Görtler vortices: vortex motion induced by wall roughness. *Phil. Trans. R. Soc.* A **335**, 51–85.

Dong, M., Liu, Y. & Wu, X. 2020 Receptivity of inviscid modes in supersonic boundary layers due to scattering of free-stream sound by localised wall roughness. *J. Fluid Mech.* **896**, A23.

Duck, P.W., Ruban, A.I. & Zhikharev, C.N. 1996 The generation of Tollmien–Schlichting waves by free-stream turbulence. *J. Fluid Mech.* **312**, 341–371.

Goldstein, M.E. 1985 Scattering of acoustic waves into Tollmien–Schlichting waves by small streamwise variation in surface geometry. *J. Fluid Mech.* **154**, 509–529.

Gulyaev, A.N., Kozlov, V.E., Kuznetsov, V.R., Mineev, B.I. & Sekundov, A.N. 1989 Interaction of a laminar boundary layer with external disturbances. *Izv. Akad. Nauk SSSR, Mekh. Zhidk. Gaza* **5**, 55–65.

Kachanov, Y.S., Kozlov, V.V. & Levchenko, V.Y. 1982 *The Apearence of Turbulence in the Boundary Layer*. Nauka.

Kerimbekov, R.M. & Ruban, A.I. 2005 Receptivity of boundary layers with to distributed wall vibrations. *Phil. Trans. R. Soc.* A **363**, 1145–1155.

Kovasznay, L.S.J. 1953 Turbulence in supersonic flow. *J. Aero. Sci.* **20** (10), 657–682.

Kravtsova, M.A., Zametaev, V.B. & Ruban, A.I. 2005 An effective numerical method for solving viscous-inviscid interaction problems. *Phil. Trans. R. Soc.* A **363** (1830), 1157–1167.

Lin, C.C. 1946 On the stability of two-dimensional parallel flows. Part 3. Stabilty in a viscous fluid. *Q. Appl. Maths* **3**, 277–301.

Messiter, A.F. 1970 Boundary-layer flow near the trailing edge of a flat plate. *SIAM J. Appl. Maths* **18** (1), 241–257.

Neiland, V.Y. 1969 Theory of laminar boundary layer separation in supersonic flow. *Izv. Akad. Nauk SSSR, Mech. Zhidk. Gaza* **4**, 53–57.

Prandtl, L. 1904 Über flüssigkeitsbewegung bei sehr kleiner Reibung. In *Verh. III. Intern. Math. Kongr., Heidelberg*, pp. 484–491. Teubner, Leipzig, 1905.

Ruban, A.I. 1984 On Tollmien–Schlichting wave generation by sound. *Izv. Akad. Nauk SSSR, Mekh. Zhid. Gaza*, 44–52.

RUBAN, A.I. 2018 *Fluid Dynamics. Part 3. Boundary Layers*. Oxford University Press.
RUBAN, A.I., BERNOTS, T. & KRAVTSOVA, M.A. 2016 Linear and nonlinear receptivity of the boundary layer in transonic flows. *J. Fluid Mech.* **786**, 154–189.
RUBAN, A.I., BERNOTS, T. & PRYCE, D. 2013 Receptivity of the boundary layer to vibrations of the wing surface. *J. Fluid Mech.* **723**, 480–528.
SCHUBAUER, G.B. & SKRAMSTAD, H.K. 1948 Laminar-boundary-layer oscillations and transition on a flat plate. Tech. Rep. NACA TR 909.
SMITH, F.T. 1979 On the non-parallel flow stability of the Blasius boundary layer. *Proc. R. Soc. Lond.* A **366**, 91–109.
STEWARTSON, K. 1969 On the flow near the trailing edge of a flat plate. *Mathematika* **16** (1), 106–121.
STEWARTSON, K. 1970 On laminar boundary layers near corners. *Q. J. Mech. Appl. Maths* **23** (2), 137–152.
STEWARTSON, K. & WILLIAMS, P.G. 1969 Self-induced separation. *Proc. R. Soc. Lond.* A **312**, 181–206.
TERENT'EV, E.D. 1981 Linear problem for a vibrator in subsonic boundary layer. *Prikl. Mat. Mech.* **45**, 1049–1055.
WU, X. 1999 Generation of Tollmien–Schlichting waves by convecting gusts interacting with sound. *J. Fluid Mech.* **397**, 285–316.
WU, X. 2001 Receptivity of boundary layers with distributed roughness to vortical and acoustic disturbances; a second order asymptotic theory and comparison with experiments. *J. Fluid Mech.* **431**, 91–133.
WU, X., ZHAO, D. & LUO, J. 2011 Excitation of steady and unsteady Görtler vortices by free-stream vortical disturbances. *J. Fluid Mech.* **682**, 66–100.
ZHUK, V.I. & RYZHOV, O.S. 1980 Free interaction and stability of boundary layer in incompressible fluid flow. *Proc. Akad. Nauk SSSR* **253**, 1326–1329.